공학박사 학위논문

The kinetics and reaction mechanism of titanium dioxide and silicon negative electrodes for lithium-ion batteries

리튬이온전지 음극 물질인 티타늄 산화물과

실리콘의 속도론과 반응 메커니즘

2015년 2월

서울대학교 대학원

공과대학 화학생물공학부

이 경 재

Abstract

The kinetics and reaction mechanism of titanium dioxide and silicon negative electrodes for lithium-ion batteries

Kyung-Jae Lee

School of Chemical & Biological Engineering

Seoul National University

Lithium-ion batteries (LIBs) are energy storage · conversion devices, which utilize reversible electrochemical reactions on anode and cathode, storing chemical energy and converting it to electrical energy. Until now, LIBs' usage has been limited to energy sources for small IT equipments. LIBs for the future, however, have far more possibilities to be applied in extended fields, such as electric vehicles, and energy storage systems. Thus, LIBs' energy density and rate performance should be enhanced. To achieve these goals, methods to use the materials with high energy densities like Si more effectively, such as improving the rate performances by coating conductive material and controlling structure of active materials, have been studied extensively. Other areas of studies, for example, understanding the reaction mechanism or segmentizing the components which can affect kinetics, are also necessary. Nevertheless, these kinds of studies are less common in the research area.

In the first part of study, Li ion diffusion in electrolyte and its effect of kinetics was investigated. The mesoporous TiO_2 was chosen because mesoporous structure is known to have facile Li ion diffusion through

electrolyte, and because other parameters related to volume expansion along the reaction can be eliminated with TiO_2 system, facilitating investigation of Li ion diffusion. 3-dimmensional mesoporous TiO_2 particles with three different pore sizes and two different particle sizes were synthesized using nano-silica as a template. Moreover, the structure of synthesized materials was analyzed with transmission electron microscopy, x-ray diffraction, small angle x-ray diffraction, and nitrogen adsorption/desorption isotherm. Using the synthesized materials, electrochemical experiments were conducted. There was no difference in electrochemical performances between the synthesized materials with 1 M concentration electrolyte. On the other hand, Li ion depletion occurs inside of the active materials depending on the size of the active materials and the pore sizes with 0.1 M concentration electrolyte. Such result reflects that the particle size and pore size are influencial parameter that affects Li ion diffusion, but their effects are negligible in 1 M concentration electrolyte. Based on the acquired results, the mathematical model with Thiele modulus was set up, and the boundaries of Li ion depletion inside of the particle was predicted using the model.

In the second part of this study, the reaction mechanism and the kinetics of Si, which has high theoretical capacity, were investigated. The reaction between Si and Li was widely reported to progress through solid-solution reaction. Recently, however, there were some reports that insist that the reaction of Li-Si is two-phase reaction, and the reaction mechanism of Li-Si requires some clarification. The main obstacle for analyzing the reaction mechanism of Li-Si is due to the amorphous structure which silicon transforms into during the reaction. Thus, routinely used analytic methods have limitations to be used in Li-Si system. In this study, the reaction between Li and Si was analyzed with electrochemical method and thermodynamic relations, which is independent of the structure of material. The result concludes that the reaction between Li and Si proceeds through two steps of

two-phase reaction. This result was confirmed by showing the trend of the diffusion coefficient change of Li in Si is similar to that of the materials with two-phase reaction. Also, it is logically more plausible to understand the reaction between Li and Si with two-phase reaction. The electrochemical performances for Si were measured with various current densities, and it was discovered that two different two-phase reactions had different kinetic properties. The cause was investigated using electrochemical impedance spectroscopy. Two resistances related to charge transfer and solid-electrolyte interphase were extracted from the impedance data, and it was found that these two resistances are not dominant parameters that determine the kinetics of two reactions. Based on these evidences, among the three kinetic parameters, diffusion in electrolyte, surface reaction, and bulk diffusion, this study concluded that the rate determining step is the diffusion in bulk phase. Furthermore, the strategy to use Si more effectively was proposed, and confirmed with experiments.

Through this study, the reaction mechanism of active material and the important kinetic parameters were clarified. These findings give some clues to effectively designing active materials depending on the environment of the reactions.

***Keywords*:** Lithium-ion batteries, Kinetics, Li-ion diffusion, Reaction mechanism, Silicon, TiO_2.

***Student Number*:** 2009-23953

Contents

List of Tables

List of Figures

Chapter 1. Introduction

1.1. Lithium-ion batteries (LIBs)

1.1.1. Background of LIBs

Lithium-ion batteries (LIBs) are energy conversion and storage devices, the difference of chemical energy between two electrodes, anode and cathode, are transformed into electric energy, the reverse direction of energy transform is also possible, using reversible oxidation/reduction reactions on each electrodes. The chemical energy (representative thermodynamic term is Gibbs free energy, *G*) and electric energy (representative thermodynamic term is electric potential, *E*) has a relation as follow:

$$\Delta G = G_{\text{anode}} - G_{\text{cathode}} = -nFE$$

As described in equation above, anode always has larger chemical energy than cathode. When the difference of chemical energy between cathode and anode decreases, which is spontaneous direction, anode is oxidized by liberating electron and lithium ion, and cathode is reduced by adapting electron and lithium ion from anode. (Discharge) On the other hand, the difference of chemical potential increases, which needs additional work, anode is reduced by adapting electron and lithium ion from cathode. (Charge)

LIBs are composed of four parts: electrolyte, separator, anode materials, and cathode materials. Electrolyte is a media for lithium ions to transport between anode and cathode. Usually, electrolyte is mixture of linear carbonate and cyclic carbonate. Linear carbonate, such as diethyl carbonate (DEC) has small viscosity, which is favorable for lithium ions to move easily in electrolyte. Whereas, linear carbonate has small dielectric constant (ε), which is unfavorable for salts to be dissociated due to large attractive interaction between cation and anion.

$$F = \frac{1}{4\pi\varepsilon_0\varepsilon}\frac{qQ}{r^2} \quad \text{(coulomb's law)}$$

where F is the magnitude of the electrostatic force, q, Q are two point charge, ε_0 is dielectric constant in vacuum, and r is the distance between two charges. To compensate large attractive interaction between cation and anion, cyclic carbonate, such as ethylene carbonate, which has high dielectric constant is mixed with linear carbonate, and it makes large amount of lithium salts can be dissociated in electrolyte. Cyclic carbonate, however, has high viscosity, which is unfavorable for lithium ions to transport. Therefore, the ratio between linear carbonate and cyclic carbonate is important.

Separator acts as physical barrier for anode and cathode to contact each other. Electric disconnection between cathode and anode in LIBs is important because if these two electrodes contact each other, short circuit is formed,

which leads major part of electrons flow through these contacts. It can cause high temperature due to joule heating.

$$Q \propto I^2 R \quad \text{(Joule's first law)}$$

where Q is generated heat, I is current, and R is resistance. Usually, separator is composed of polyolefin such as polyethylene (PE), and polypropylene (PP) with porous membrane structure. This porous structure can facilitate the transport of ions in electrolyte.

Anode and cathode materials are the host of lithium ion and electron. The chemical energy of lithium in anode and cathode is different, and this difference is driving force for spontaneous oxidation/reduction reactions at each electrodes. The chemical potential of lithium depends on the host materials. In anode materials, they can be classified with the reaction mechanism: insertion, conversion, and alloying mechanisms. The representative materials with insertion mechanism are graphite and TiO_2. And, the examples of the materials with conversion mechanism are various metal oxides, such as iron oxide, cobalt oxide, and manganese oxide. Finally, the examples of the materials with alloying mechanism are Si, Sn, and Ge. In the case of cathode materials, on the other hand, they can be classified with the structure of the active materials: layered, spinel, olivine structures. The materials with layered structure have two dimensional diffusion path for Li,

and they have representative stoichiometry with '$Li_1M_1O_2$', where M stands for metal. The examples of the materials with layered structure are $LiCoO_2$, and $LiNiO_2$. In the case of the materials with spinel structure, they have three dimensional path for Li and have typical molecular formula is '$Li_1M_2O_4$'.The example is $LiMn_2O_4$. Finally, the materials with olivine structure have one dimensional diffusion path for Li, and their molecular formula is '$LiMPO_4$'. The examples are $LiFePO_4$ and $LiMnPO_4$.[1,2]

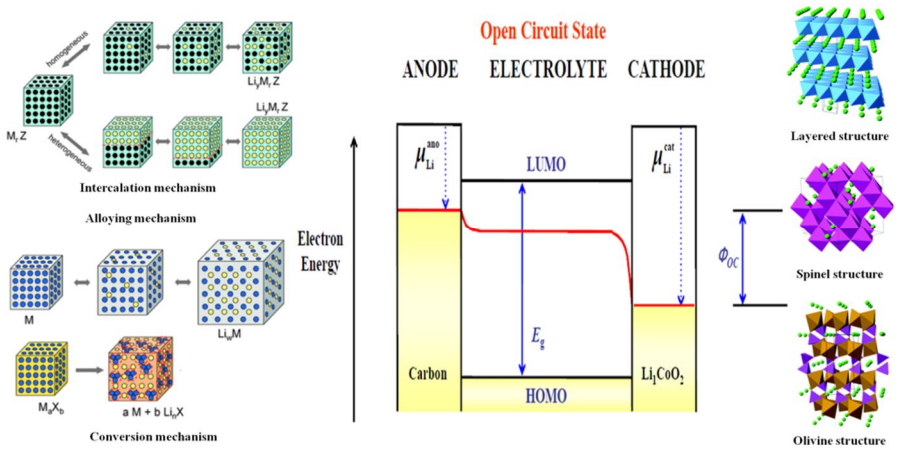

Figure 1.1. Electron energy diagram of LIBs and classified anode and cathode materials. (Adapted from the M.S. Islam et al., Chem. Soc. Rev., **2014**, 43, 185; M.R. Palacin, Chem. Soc. Rev. **2009**, 38, 2565)

1.1.1. Past, present and future of LIBs

In the late 1970's, TiS_2/Li cell, which can be considered as the first LIB, was proposed by Whittingham from Exxon, but it suffered from various problems, such as Li plating. These problems were the obstacles that make TiS_2/Li cell be commercialize. After several years, R. Yazami from INPG found the fact that Li can reversibly intercalated/deintercalated to graphite with electrochemical method.[3] In addition, J.B. Goodenough found that layered oxide ($LiCoO_2$) also can store Li reversibly within its structure.[4] SONY combined these two materials, and made the first commercialized LIB in 1991. These materials can store Li in safe way, thus, LIB from SONY can avoid from the problems which the previous LIB had. These LIBs had 2~3 times larger energy densities than existing secondary batteries that present, such as lead-acid cells, and Ni-Cd cells. Furthermore, LIBs have little self-discharge and memory effect, which conventional secondary batteries in the past had, thus they have been applied to various small IT equipments, such as lab-top computers and cellular phones, which need frequent charging and discharging.

LIBs for future have infinite possibilities to be applied to the fields beyond so far. Wall street journal, which is an influential newspaper, reported five technologies that can change everything as follows: (1) space based solar

power, (2) advanced car batteries, (3) utility storage, (4) carbon capture and storage, and (5) next-generation biofuels.[5] The batteries for electric vehicles and energy storages, as mentioned above, are representative examples of future LIBs. They require improved energy densities and rate performance than those of LIBs until now. Therefore, there is an ongoing effort to enhance energy densities and improve the kinetics, and meaningful results have been made.[6]

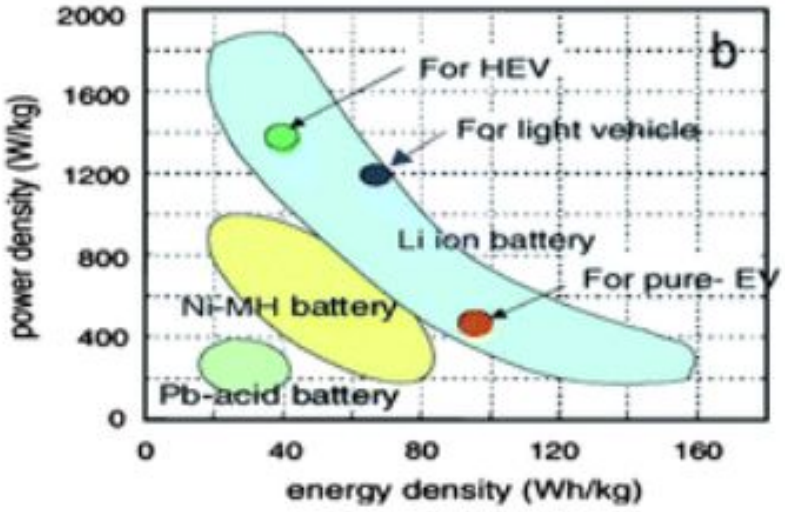

Figure 1.2., Ragone plot (Adapted from D. Aurbach et al., Energy Environ. Sci., **2011**, 4, 3242)

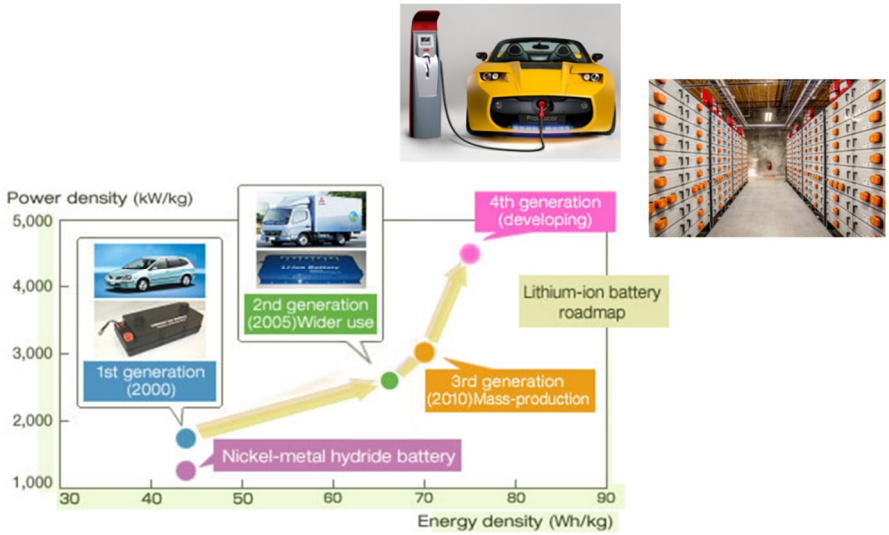

Figure 1.3. The past, present, and future of LIBs (Adapted from http://futurehumanevolution.com/todays-technology/disruptive-technology-energy-storage;http://cleantechnica.com/2013/06/09/5-mw-lithium-ion-energy-storage-system-unveiled-in-oregon-will-provide-storage-for-intermittent-renewable-energy-sources/; http://www.hitachi.com/environment/showcase/solution/mobility/lithiumion.html)

1.2. Recent issues on LIBs

1.2.1. About energy density

The high energy density is one of important and required property which the future LIBs should have. The energy density is the amount of energy stored in the system. It can be divided into two types; volumetric energy density and gravimetric energy density. The volumetric energy density is the amount of energy stored in a unit volume, and has a dimension of J m^{-3}. It depends on the various parameters, such as the kinds of active material, the size of active material, mass ratio of active materials, conducting agent, and binder, and porosity of the electrode. Therefore, this value can be regulated with the manufacturing process, which can change the parameters mentioned above, even with fixed mass ratio of the component and specified active material. On the other hand, when the mass ratio of the components is fixed, then, the gravimetric energy density solely depends on the kinds of active material; this value is the amount of energy stored in a unit mass, and has a dimension of J kg^{-1}. In following part, only the gravimetric energy density will be considered. Especially, specific capacity, which is the amount of coulombs stored within specific voltage window in a unit mass along the various anode active materials, the problems related to the active materials, and various strategies

to solve such problems will be introduced.

The anode materials are classified with its reaction mechanism; intercalation, conversion, and alloying mechanism. Among anode materials, the materials which use intercalation mechanism, such as graphite TiO_2 and $Li_4Ti_5O_{12}$ have relatively small specific capacity. Li intercalation with maintaining its own structure has limitation in the number of active sites, resulting in small specific capacity. In this kind of materials, amorphization is frequently used to increase specific capacity; hard carbon, or amorphous TiO_2 have larger specific capacity than graphite and c-TiO_2.[7,8] Amorphous structure has additional sites for Li intercalation, such as defect sites. Thus amorphous materials can have poor coulombic efficiency due to irreversibility of such additional sites. On the other hand, the materials which use conversion mechanism and alloying mechanism, such as FeO_x, CoO_x, MnO_x for conversion mechanism, and Si, Sn, and Ge for alloying mechanism, have large specific capacities over 1000 mAh g^{-1}, and therefore, they are counted as possible candidates for future anode material for LIBs.[9-11] In this case, the reaction with Li deforms its original structure, and new bonds are formed within active materials. Therefore, its reaction kinetics are usually slower than that of materials with intercalation mechanism.[12] Furthermore, such materials suffers from large volume expansion along the reaction with Li.[13,

14] This volume expansion is inevitable due to intrinsic volume of Li; the more Li reacted, the more volume expansion happens. And, these materials usually have low intrinsic electric conductivities.[15] Therefore, various trials have been conducted to improve the electrochemical performance from such problems. The first strategy, which is the most frequently tried, is nano-architecturing.[16-20] Nano-structure can alleviate the problems related to slow kinetics due to decreased diffusion path. Furthermore, nano-structure can also relieve the stresses originated from volume expansion along the reaction effectively, resulting in reducing the possibility of electric disconnection between active materials and current collector. Various nano-structured materials are introduced as an example in Figure 1.4. Another strategy is coating with conductive materials, such as carbon.[21-23] The coating with conductive material can enhance electric conductivity in the electrode, and relieving the problems related to low electric conductivity. In addition, coating on the active material also can help to maintain its original structure, resulting in reducing electric disconnection between active materials and current collector.[24] These trials effectively solve the problems, therefore, many groups have reported many cases with high specific capacities, and even at higher current densities.

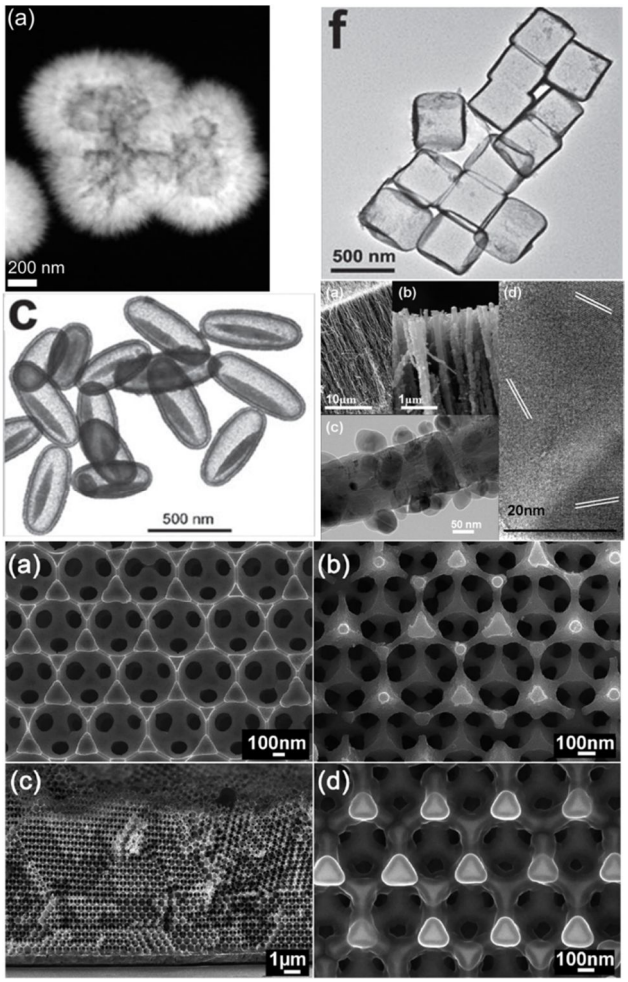

Figure 1.4., Various nano-structured anode materials.(Adapted from the Y.S. Huh et al., Adv. Mater., **2013**, 25, 6250; X.W. Lou et al., J. Am. Chem. Soc. **2011**, 133, 4738; L.A. Archer et al., Adv. Mater., **2007**, 19, 3328; N. Kumta et al., ACS Nano, **2010**, 4, 223; P.V. Braun et al., Nano Lett., **2012**, 12, 2778)

1.2.2. About rate performance

Good rate performance is also important and required property for future LIBs, like high energy density. To achieve good rate performance, the kinetics of the active material should be understood. The kinetics can be divided into three parts: Li ion diffusion through electrolyte, electrochemical reaction at interface of the active materials, and Li diffusion through bulk phase of active materials. In general, the electrochemical reaction at interface of the active materials and Li diffusion through bulk phase is considered as a rate determining steps in the kinetics of LIBs. Therefore, many efforts to differentiate which step is rate determining step between bulk diffusion and surface reaction have been done [25], and various methods have been tried to enhance surface reaction or bulk diffusion. The surface reaction depends on various properties of surface of active materials, such as conductivity, and phase of active materials. Therefore, coating with conductive material, or surface amorphization have been tried to improve surface reaction.[26,27] And, bulk diffusion usually depends on structure of bulk phase, therefore, doping in bulk phase, amorphization of bulk phase or ion exchange of specific sites have been tried to improve bulk diffusion. Unlike the surface reaction and the bulk diffusion, the diffusion through electrolyte is considered less important step in the kinetics. The diffusion in electrolyte is, however,

important in high current densities. If Li ion diffusion in electrolyte cannot catch up the rate of electrochemical reaction, some part will be existed without electrochemical reaction, resulting in inefficient active material utilization. The main stream to enhance the diffusion in electrolyte is making mesoporous material.[28,29] The mesoporous material has large surface area, thus, the accessibility of Li ion toward the active materials can be enhanced. In recent studies, more improved mesoporous structure, such as ordered mesoporous structure, is used to further enhance Li ion diffusion through electrolyte.[30,31] By these strategies, kinetics in LIBs are well improved, and shows good rate performance even at high current densities.(Figure 1.5.) Therefore, it cannot be emphasized enough that understanding of kinetics is important to enhance rate performance of LIBs.

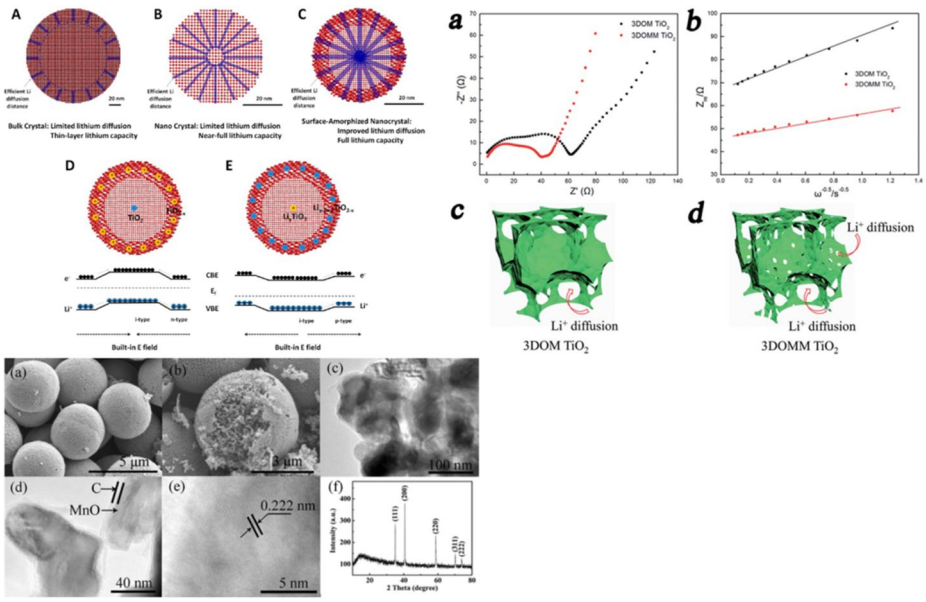

Figure 1.5., Examples that show enhanced kinetic properties with surface treatment and structure control. (Adapted from the B.L. Su et al,, J. Mater. Chem. A, **2014**, 2, 9699; X. Chen et al., Nano Lett., **2013**, 13, 5289; W. Liu et al., CrystEngComm., **2014**, 16, 1802)

1.2.3. About reaction mechanism

The mechanism of the reaction between Li and active materials can be divided into two types; solid-solution reaction and two-phase reaction. Two reaction mechanisms can be understood differently in the thermodynamic respects.

The materials with solid-solution reaction have continuous active sites along the energy of Li. Therefore, the concentration of Li, or the energy of Li in the host material can be changed continuously. (The concentration of Li and the potential has relation of $\mu_{\mathrm{Li}} = \frac{\partial G_{\mathrm{Li}}}{\partial n_{\mathrm{Li}}} = RT \ln a_{\mathrm{Li}} = RT \ln (\gamma_{\mathrm{Li}} C_{\mathrm{Li}})$, where, μ_{Li} is chemical potential of Li, G_{Li} is Gibbs free energy of Li, R gas constant, T is temperature, a_{Li} is activity of Li, γ_{Li} is activity coefficient of Li, and C_{Li} is concentration of Li) The progress of the reaction in the materials with solid-solution reaction can be easily understood in the equations below: [32]

$$\delta\ \mathrm{Li} + \mathrm{H} \rightarrow \mathrm{Li}_{\delta}\mathrm{H}$$

$$\delta\ \mathrm{Li} + \mathrm{Li}_{\delta}\mathrm{H} \rightarrow \mathrm{Li}_{2\delta}\mathrm{H}$$

$$\vdots$$

$$\delta\ \mathrm{Li} + \mathrm{Li}_{1-\delta}\mathrm{H} \rightarrow \mathrm{LiH}$$

$$\mathrm{Li} + \mathrm{H} \rightarrow \mathrm{LiH}$$

where H stands for the host. As stoichiometry of Li in the host increases, the

activity of Li in the host also increases as described above. Due to continuous increase of Li activity, therefore, lithiation/delithiation profile has sloping tendency. It can be explained with Gibbs free energy diagram in Figure 1.6.

In the case of the materials with two-phase reaction, it shows different reaction progress with solid-solution reaction. The equations for the progress in the case of the materials with two-phase reaction are as follows:

$$\delta\,\mathrm{Li} + \mathrm{H} \rightarrow \delta\,\mathrm{LiH} + (1-\delta)\mathrm{H}$$

$$\delta\,\mathrm{Li} + [\delta\,\mathrm{LiH} + (1-\delta)\mathrm{H}] \rightarrow 2\delta\,\mathrm{LiH} + (1-2\delta)\mathrm{H}$$

$$\vdots$$

$$\delta\,\mathrm{Li} + [(1-\delta)\,\mathrm{LiH} + \delta\,\mathrm{H}] \rightarrow \mathrm{LiH}$$

$$\mathrm{Li} + \mathrm{H} \rightarrow \mathrm{LiH}$$

During the progress, same reaction happens. It can be considered that the reaction sites for Li have same energy level. Therefore, as the reaction goes on, the composition of two phases changes with lever rule. [33] And, the activity of Li is constant, thus, lithiation/delithiation profile has flat plateau. It can also be explained with Gibbs free enrgy diagram in Figure 1.6.

The simple method to figure out what the reaction mechanism of the active material is, is to confirm the shape of lithiation/delithiation profile; if the lithiation/delithiation profile is sloping shape, the active materials go through solid-solution reaction, and if the profile shows flat plateau, then, the reaction mechanism of the active material is two-phase reaction. In some cases,

however, this relation is contradicted. Therefore, careful approach to determine the reaction mechanism is necessary.

Understanding the reaction mechanism can be considered to be unnecessary. Because confirming the reaction mechanism is just ‘confirming the reaction mechanism’. However, choosing the analytic method is affected by the reaction mechanism; measuring diffusion coefficient of the materials with two-phase reaction and with solid-solution reaction should be differentiated. Furthermore, it has its own scientific meaning.

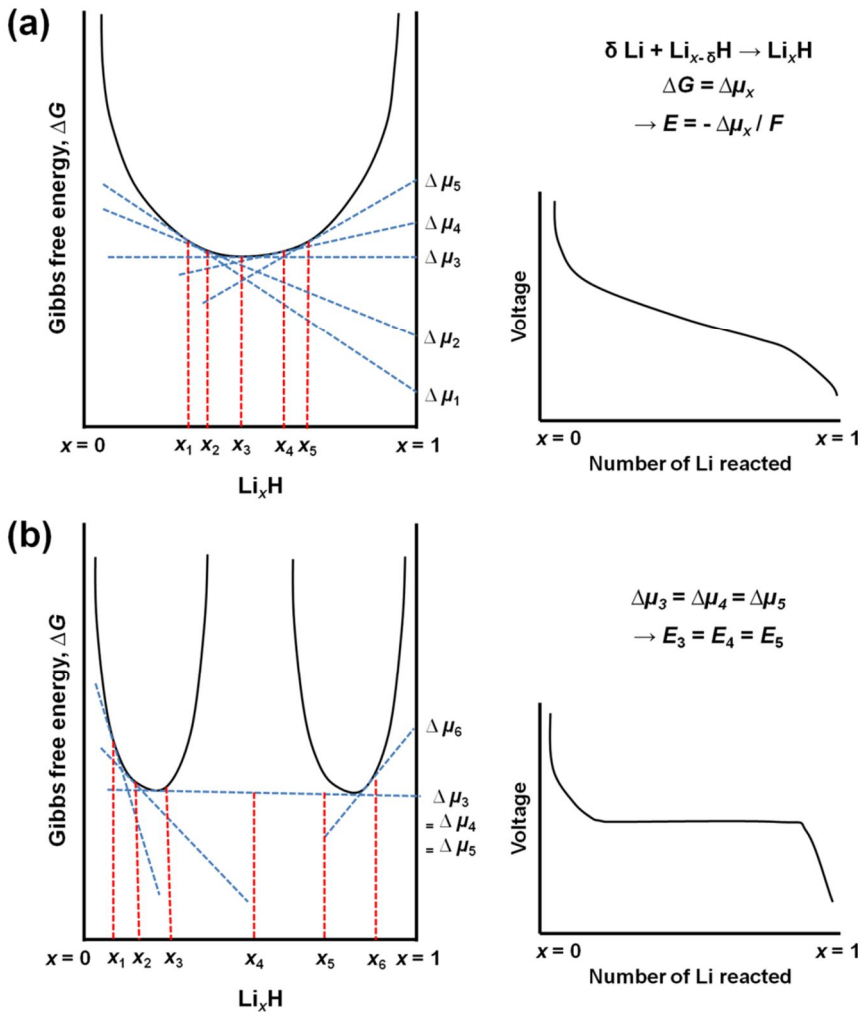

Figure 1.6. Gibbs free energy diagram for the case of (a) solid-solution reaction and (b) two-phase reaction.

1.3. Objectives of this dissertation

Through this study, I tried to understand the kinetics of anode materials in LIBs with two separated parts: one is about Li ion diffusion through electrolyte and another is about surface reaction or bulk diffusion. Furthermore, I tried to reveal the reaction mechanism of Si, which is still unclear.

In the part of studying Li ion diffusion in electrolyte, 3-dimensional ordered (3DOm) mesoporous TiO_2 was chosen as a model system. Because TiO_2 can be considered to be free from volume change along the reaction, it can eliminate other unnecessary possibilities that related to structure change of the active material. Furthermore, TiO_2 can stand high current densities where the importance of Li ion diffusion in electrolyte is amplified. Thus TiO_2 can be an ideal material to study Li ion diffusion in electrolyte. And, mesoporous structure was chosen due to the fact that many researches are going on using mesoporous structure, recently. In spite of such vigorous studies on mesoporous structure, there are little studies that investigating the effect of the parameters, such as particle size, pore size, porosity, and tortuosity, on the electrochemical performance. Therefore, I tried to find how these parameters affect to Li ion depletion inside of mesoporous meaterials, and further tried to make a model that predict the relation

between the particle size and the current density that Li ion starts to be depleted.

In another part of this study, I tried to investigate the reaction mechanism and the kinetics of Li-Si system. Si is chosen as the material to be studied, because it is considered as a promising anode material for future LIBs due to its high theoretical capacity. In addition, the reaction mechanism of Li and Si system is still unclear, which makes this system be interesting. Electrochemical method and thermodynamic relations were used to figure out how Si and Li reacts each other. And then, the kinetic properties of the steps in the reaction between Li and Si were investigated with various electrochemical methods, such as differential capacity profiles and electrochemical impedance spectroscopy. Furthermore, new strategy to use Si more effectively was proposed based on the information acquired from above investigations.

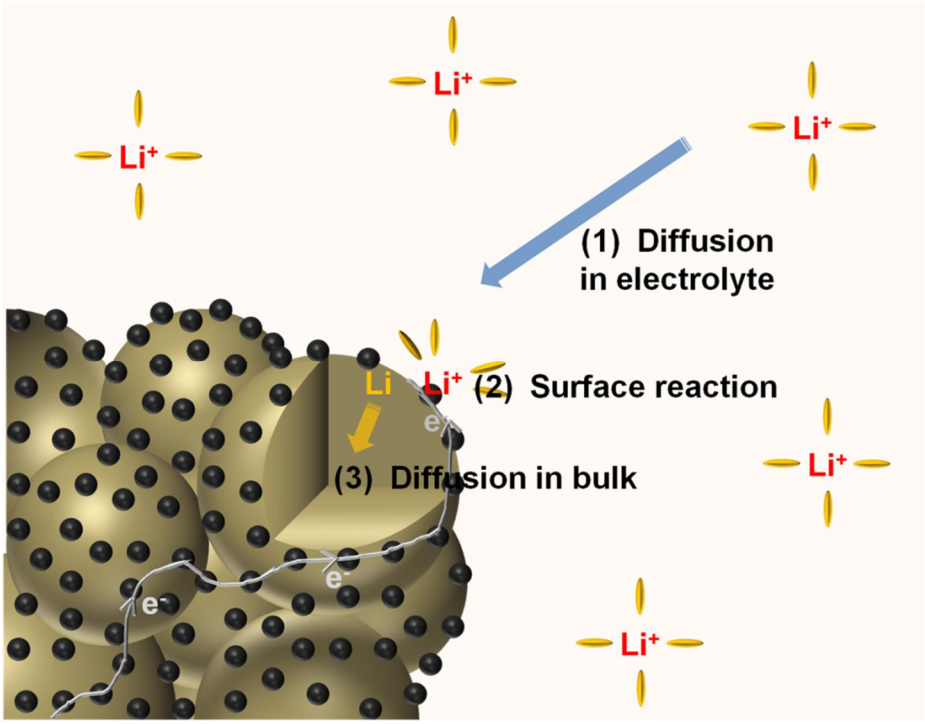

Figure 1.7. The scheme of this dissertation.

Chapter 2. Li ion diffusion through the pores in mesoporous structures

2.1. Introduction

In order to improve kinetics, many studies have been done to understand the rate limiting step. The kinetics can be categorized into three groups; diffusion in bulk, surface reactions, and diffusion in electrolyte. In general, diffusion in bulk and surface reactions are treated as rate determining steps in LIBs. Therefore, comprehensive studies have been done to understand diffusion in bulk and surface reactions, and the methods to improve those reactions, such as carbon coating, and amorphization of active materials, have been proven to work. On the other hand, diffusion in electrolyte is also an important part of kinetics; if diffusion of Li salt cannot supply enough reactants for the electrochemical reactions, salt depletion occurs, and active materials cannot be utilized. Most studies to improve the diffusion in electrolyte have been focused on making mesoporous materials. Such materials have pores interconnected inside the particle, facilitating Li ion diffusion, and increasing contact area between electrolyte and active materials. Recently, ordered mesoporous materials, an extension to ordinary

mesoporous materials, were applied to further improve Li ion diffusion through active materials. These kinds of approaches, intuitively, seem to improve Li ion diffusion using ordered pores, which results in improved power performance. However, studies on the degree of kinetic benefit the ordered pores have over the random pores, or the effect of pore size or the particle size of mesoporous materials on electrochemical performance, are insufficient.

In this study, 3-dimensional ordered mesoporous (3DOm) titania particles with different pore sizes (14 nm 24 nm and 44 nm) and different particle sizes (approximately 500 nm and 1000 nm) were synthesized using closed-packed silica particles as a hard template, while the electrochemical performance at two different concentrations of Li salt in electrolyte was examined. In addition, nonporous and randomly aggregated titania particles were also examined to see the effect of existence of mesopores and ordered pores on the electrochemical performance. titania is known to have little volume expansion during the reaction with Li ion, therefore it is a good system to study the effect of changing pore sizes and particles sizes on the electrochemical performance. The experimental values are compared with mathematical model which is frequently used in porous catalyst system, allowing extended insights into the effects of changed parameters on 3DOm

titania particles' electrochemical performance.

2.2. Experimental

2.2.1. Materials synthesis

Close-packed silica particles were synthesized as a hard template for 3DOm titania particles, following a published procedure.[34-36] Deionized (DI) water (150 ml) and L-lysine (0.15 g, Sigma Aldrich) were vigorously stirred for 15 minutes. Afterwards, tetraethylorthosilicate (TEOS, 20.8 g, Samchun Chemical, Korea) was added into the solvent, and was further stirred for 15 minutes at room temperature. The solvent was then transferred to a bottle bath which was kept at 90 °C, and stirred for 48 hours with perfect sealing. TEOS (20.8 g) was added several times at timed intervals for 48 hours and the amount of TEOS addition into the solvent determined the size of the finished silica particles. After the silica particles were synthesized, the solution containing the silica particles was placed in a convection oven at 85 °C to evaporate the solvent and allow for packing of the silica particles into a close-packed structure. During this process, avoiding unnecessary vibrations from the environment is critical to forming close-packed silica.

Synthesis of 3DOm titania nanoparticles was achieved with modification following a published procedure. [37] In a Teflon-lined autoclave reactor, 2.2 g (or 4.4 g) of Ti (IV) oxysulfate (Sigma Aldrich), 18 g of anhydrous ethanol (Samchun, Korea), and 4 g of the

closed-packed silica were mixed and hydrothermally reacted at 115 °C for 48 hours. During this process, titania particles were synthesized inside the pores of closed-packed silica, creating a 3-dimensionally connected structure. The amount of Ti precursor added determined the size of the mesoporous titania particles. After the reaction, the bulk of close-packed silica embedded with titania particles were sonicated to remove incomplete 3DOm titania particles on the surface. The resulting solution was dissolved in 1 M of KOH solution to remove the silica particles, and the remaining solution containing 3DOm titania particles was neutralized to pH 7 with repeated DI washing. As a control sample, commercial anatase (Alfa Aesar) was purchased.

2.2.2. Characterizations and electrochemical test

The crystallographic phases of synthesized 3DOm titania samples and commercial titania were identified with X-ray diffraction (XRD, Rigaku, D-MAX2500-PC, Japan) using Cu Kα radiation (λ = 1.5412 Å, 40kV, 100 mA). The morphologies of the samples were observed by field emission scanning electron microscope (FE-SEM, JEOL, JSM-6701F), and transmission electron microscope (TEM, FEI, Tecnai F20). The periodicity of the close packed SiO_2 particles and 3DOm titania nanoparticles was confirmed with small angle X-ray scattering (SAXS, Rigaku, SmartLab, Japan) using Cu Kα radiation (λ = 1.5412 Å, 45kV, 200 mA). The nitrogen adsorption-desorption isotherms were measured at 77K on a Belsorp Mini-II. Samples were degassed at 150 °C under vacuum ($p < 10^{-5}$ mbar) for 12 hours. Pore size distribution curves were obtained from the adsorption branch using the Barrett-Joyner-Halenda (BJH) method. The specific areas of the samples were obtained from the Brunauer-Emmett-Teller (BET) method.

Active material (70 wt. %), super P carbon black (15 wt. %), and polyvinylidene fluoride (15 wt. %, PVDF) were mixed with *N*-methyl-2-pyrrolidone solvent until a slurry mixture was made. The prepared slurry was spread onto a copper foil, which functions as a current collector, using

the doctor blade method. The prepared electrode was vacuum-dried at 120 °C for 8 hours, and then transferred to an argon-filled glove box. The cell was assembled into a CR2016-type coin cell. The electrolyte used was 1 M $LiPF_6$ with ethylene carbonate / diethyl carbonate (EC: DEC = 1:1, v/v, Panatech, Korea), and the separator was a polyolefin microporous film from SK Innovation. In the case of 0.1 M $LiPF_6$ electrolyte, ordinary 1 M $LiPF_6$ electrolyte was diluted to one tenth of the concentration with an EC/DEC solution (Panatech, Korea). Li metal was used as a counter electrode. The galvanostatic charge / discharge tests were measured with WBCS3000 cycler (Won-A tech, Korea) with a constant temperature of 25 °C. The voltage window for electrochemical measurements was from 1.0 to 3.0 V, and current densities were varied from 1 C to 60 C. (1 C = 167.5 mA g^{-1})

2.3. Results and discussion

2.3.1. Preparation and characterization of 3DOm titania

Monodisperse silica particles with size ranges of several tens of nanometers were synthesized by following published procedures. [34-36] The SEM images showed monodisperse and close-packed silica particles with sizes varied from 20 nm to 67 nm, which were controlled by use of the amount of Si precursor added (Figure 2.1); the larger amount of Si precursor produced the larger particle size. The SEM images also confirmed that slow solvent evaporation provided close-packed silica particles. This periodicity was confirmed by SAXS measurement (Figure 2.2). The diffraction peaks from the close-packed of silica particles (20 nm) at 0.58 and 0.94 2-theta degrees correlate to (111) and (220) planes of a face-centered cubic (fcc) periodicity whose sizes are approximately 19 nm. In addition, the diffraction peaks from the close-packed of silica particles (40 nm) at 0.30 and 0.50 degrees correlate to the (111) and (220) planes with a fcc periodicity having a size of 36 nm. These demonstrate that the sizes of periodicity are similar with those of the silica particles determined by SEM measurements. [34-36]

In an attempt to realize the systematic control of a structurally well-defined titania material, a hard template method that can define the size of mesopore of the produced material (here 3DOm titania) by the choose of the size of the

parent material (here close-packed silica particle) was applied. In addition, through careful control of synthetic conditions, the size of the 3DOm titania particles was tuned. Accordingly, 3DOm titania particles were synthesized using three different sizes of silica spheres (20 nm, 40 nm and 67 nm) as hard templates via an infiltration hydrothermal reaction and a subsequent removal of silica particles.[37] XRD analyses of as made 3DOm titania particles show a crystalline material that consists in anatase phase and the crystallite sizes for the samples determined by the Scherrer equation increase gradually from 7.5 nm to 12 nm along the silica size increases. (Figure 2.3) The empty space where titania grows is proportional to the size of silica particles used as hard template, therefore, the crystallite size of titania is proportional to the size of silica particles. In addition, the SEM images shown in Figure 2.4 confirmed the successful synthesis of 3DOm titania particles.

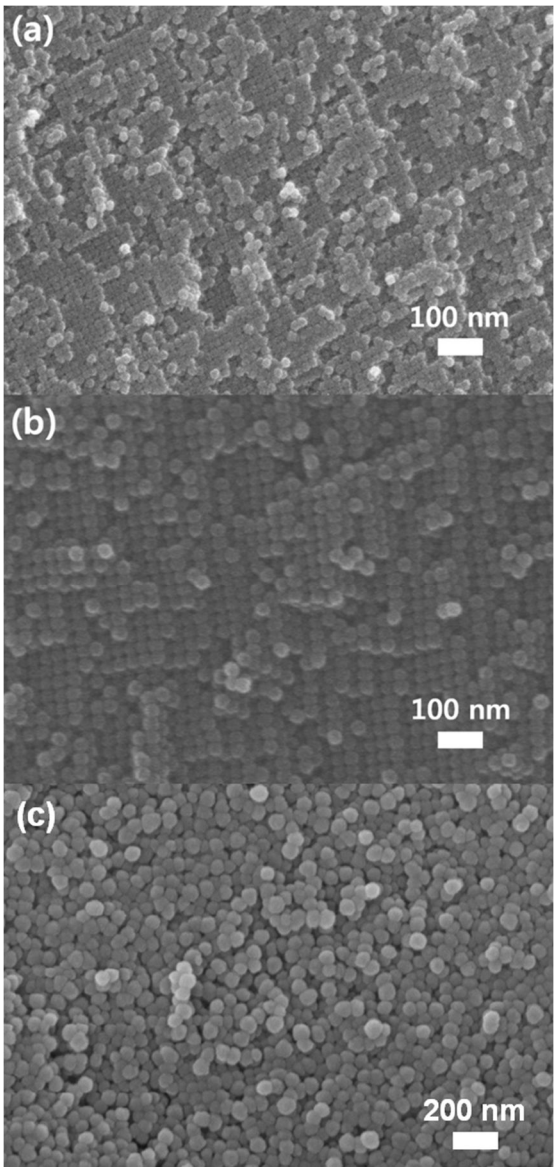

Figure 2.1. SEM of close-packed silica particles: (a) silica with 20 nm, (b) SiO_2 with 40 nm, and (c) silica with 67 nm.

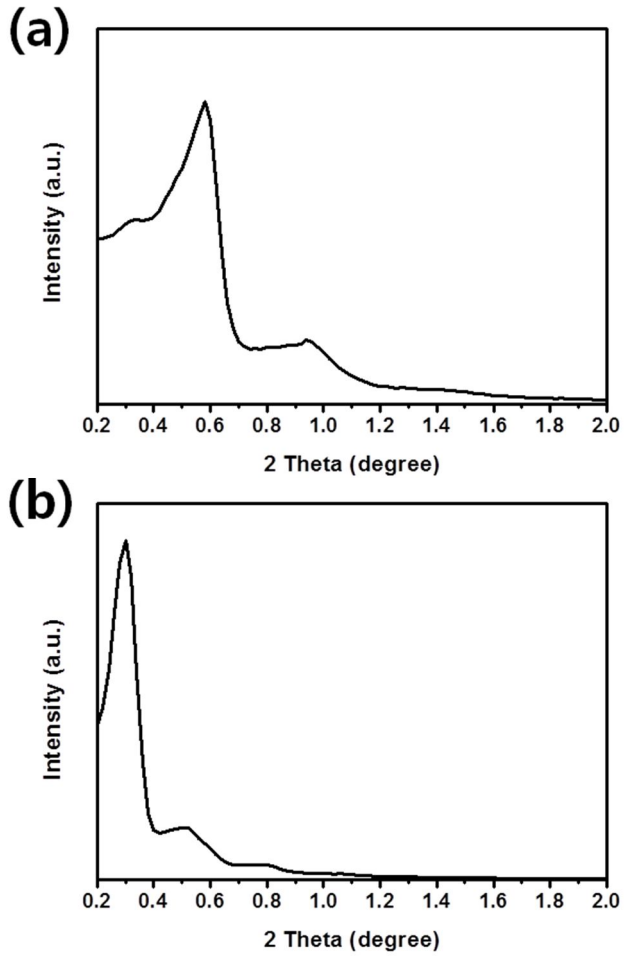

Figure 2.2. SAXS of close-packed silica particles: (a) silica with 20 nm, (b) silica with 40 nm.

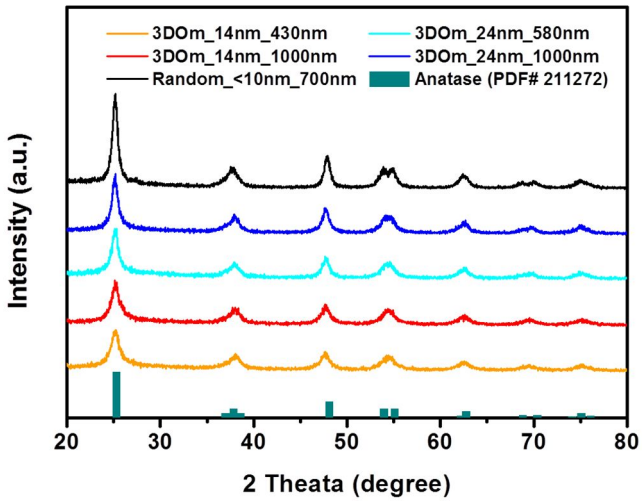

Figure 2.3. XRD patterns of the samples, and reference anatase (PDF# 211272).

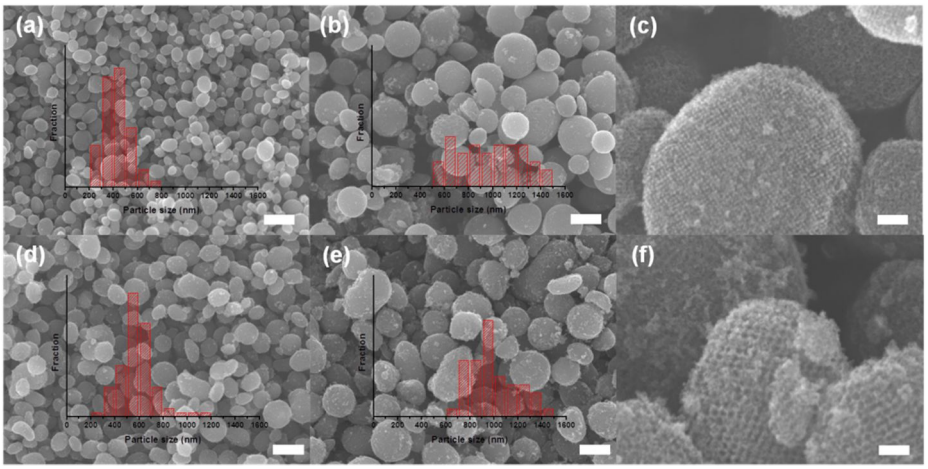

Figure 2.4. SEM images of 3DOm samples and size distribution; (a) 3DOm_14nm_430nm, (b) 3DOm_14nm_1000nm, (c) high magnification image of 3DOm_14nm_430nm, (d) 3DOm_24nm_580nm, (e) 3DOm_24nm _1000nm, and (f) high magnification image of 3DOm_24nm_580nm. The scale bars in (a), (b), (d), and (e) are 1 μm, and the scale bars in (c) and (f) are 100 nm.

3DOm titania particles with sizes of around 500 nm and 1000 nm were synthesized by adjusting Ti precursor amounts used; when the various amounts (2.2 g and 4.4 g) of Ti precursor were used, the smaller (2.2 g) and larger (4.4 g) amounts of Ti precursor provided around 500 nm (actually 430 ± 110 nm and 580 ± 148 nm for 3DOm titania particles from 20 nm and 40 nm silica spheres, respectively, Table 2.1) and around 1000 nm (actually 970 ± 265 nm, 985 ± 190 nm, and 1054 ± 186 nm for 3DOm titania particles from 20 nm, 40 nm, and 67 nm silica spheres, respectively, Table 2.1) determined by SEM measurements, respectively. In addition, high magnification SEM images of the 3DOm titania particles show voids where silica template existed prior to removal.

In addition, the ordered arrangement of the pores within the 3DOm titania particles were also confirmed using SAXS (Figure 2.5). Furthermore, when the periodicities in 3DOm titania were compared with that of silica, it was found that the periodicities of silica particles used (20 nm and 40 nm) was completely transferred to those of 3DOm titania particles. The periodicities of the pores were reconfirmed by TEM images of the 3DOm titania particles as shown in Figure 2.6. The TEM images also showed the existence of similar sized, monodispersed pores in the 3DOm titania compared to those

of the parent silica particles. These pores also were also well aligned. Existence of the anatase phase was also confirmed through fast-fourier transform (FFT) patterns, showing the existence of the (101) and (200) planes of the anatase phase in the Figure 2.6(c) and 2.6(f). Furthermore, the uniform size of the pores was also determined and confirmed using nitrogen sorption isotherms and the BJH analysis (Figure 2.7 and 2.8). Based on the maximum height point of the BJH pore size distributions, the 3DOm titania particle synthesized from 20 nm, 40nm and 67 nm silica particle was found to have 14 nm, 24nm and 44nm in pore size, respectively. Therefore, five 3DOm titania particles with the same crystallinity and morphology except different particle sizes (around 500 nm and 1000 nm) and pore sizes (hereafter, maximum height points of the BJH pore size distributions of 14 nm, 24nm and 44 nm will be used as the pore size of the 3DOm titania particles) were successfully synthesized. Based on differences for particle sizes and pore sizes, it is suggested that naming of the four different 3DOm titania as followed 'structure_pore size_particle size' (for 3DOm titania particles with 970 ± 265 nm and 985 ± 190 nm in sizes, it is referred to as 1000 nm for both samples): 3DOm_14nm_430nm, 3DOm_14nm_1000nm, 3DOm_24nm _580nm, 3DOm_ 24nm_1000nm and 3DOm_ 44nm_1000nm.

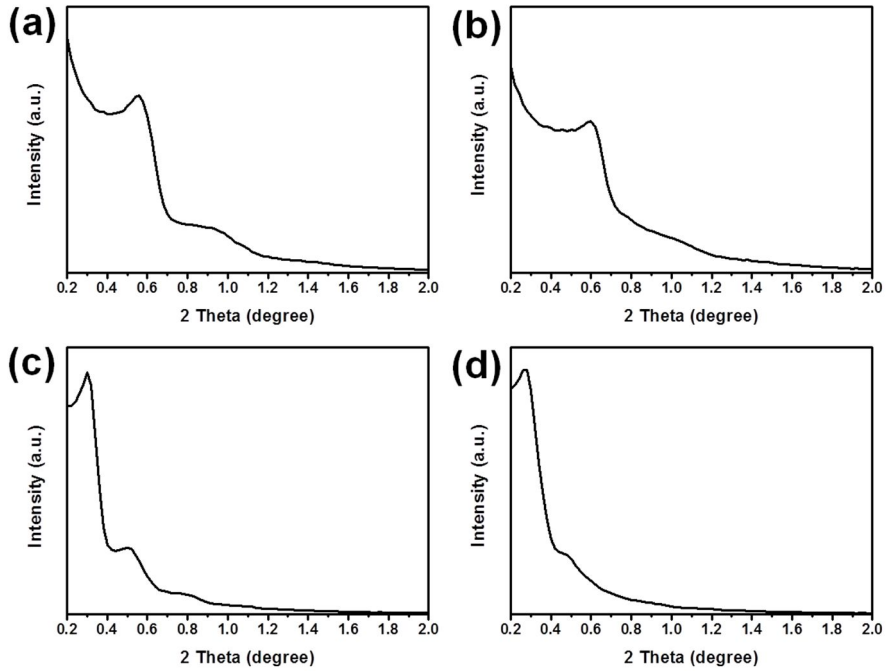

Figure 2.5. SAXS of 3DOm samples; (a) 3DOm_14nm_430nm, (b) 3DOm_14nm_1000nm, (c) 3DOm_24nm_580nm, and (d) 3DOm_24nm _1000nm.

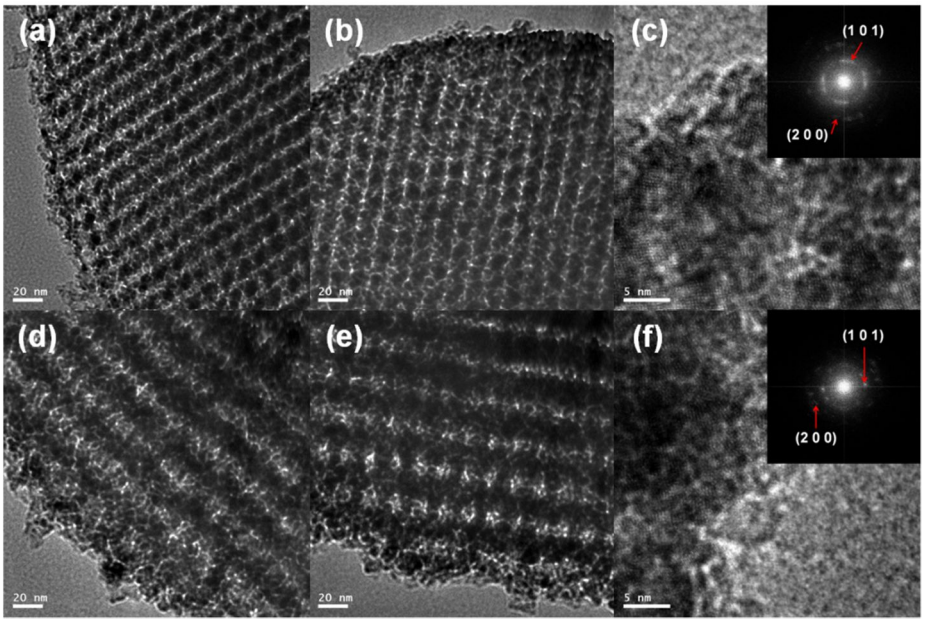

Figure 2.6. TEM images of 3DOm samples; (a) 3DOm_14nm_430nm, (b) 3DOm_14nm_1000nm, (c) high magnification image of 3DOm_14nm_1000nm, (d) 3DOm_24nm_580nm, (e) 3DOm_24nm_1000nm, and (f) high magnification image of 3DOm_24nm_1000nm. Insets in (c) and (f) are fast fourier transform (FFT) image of (c) and (e), and indexed planes are from anatase.

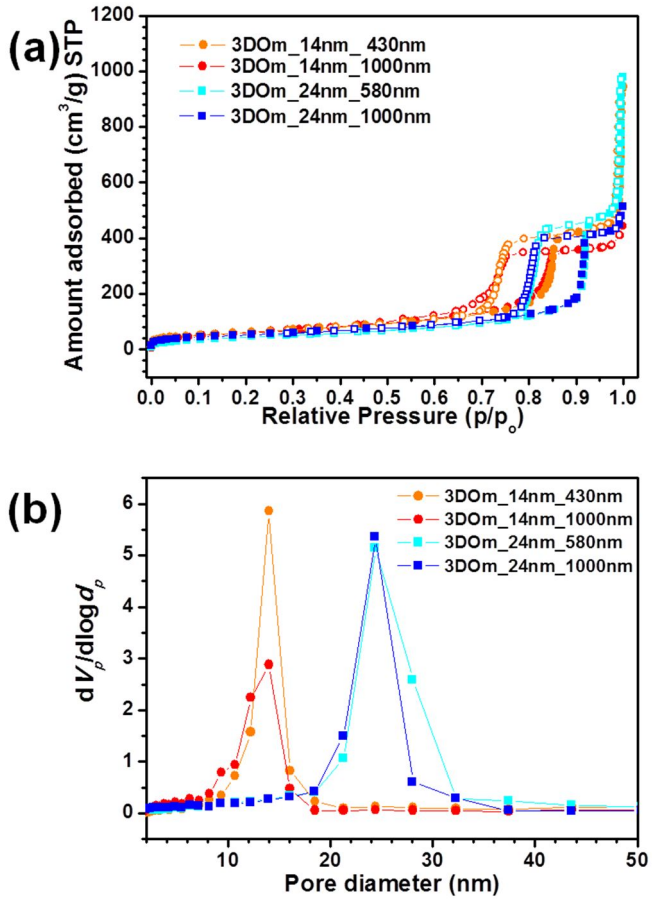

Figure 2.7. (a) The nitrogen sorption isotherms and (b) pore distributions analyzed by BJH method of the samples.

The physical properties of 3DOm_44nm_1000nm are presented in Figure 2.8. Their average particle size and pore size distributions are estimated from SEM and BJH analysis which is same methods with other 3DOm samples. And to confirm the effect of pores on the electrochemical performance, nonporous titania was synthesized without silica hard template. It has relatively large surface area due to its small particle size (350 nm), but due to lack of hard template, its total pore volume is very small compared to other samples (0.16) Since changes in crystalline size of the active material can lead to significant changes in electrochemical performance, a commercial anatase titania having a crystalline size (12 nm) determined by the Scherrer equation similar to that of the synthesized 3DOm titania (8 nm) was purchased and used as a control group.[38-40] The commercial titania showed the average particle size of around 700 nm and contained a broad pore distribution under 10 nm as shown in Figure 2.9. No XRD patterns were visible when SAXS measurements were used, implying that the primary particles are aggregated without any regularity. Based on these properties, the commercial sample was labeled 'Random_<10nm_700nm'. The physical properties of the synthesized four 3DOm titania particles and the commercial anatase sample are tabulated in Table 2.1.

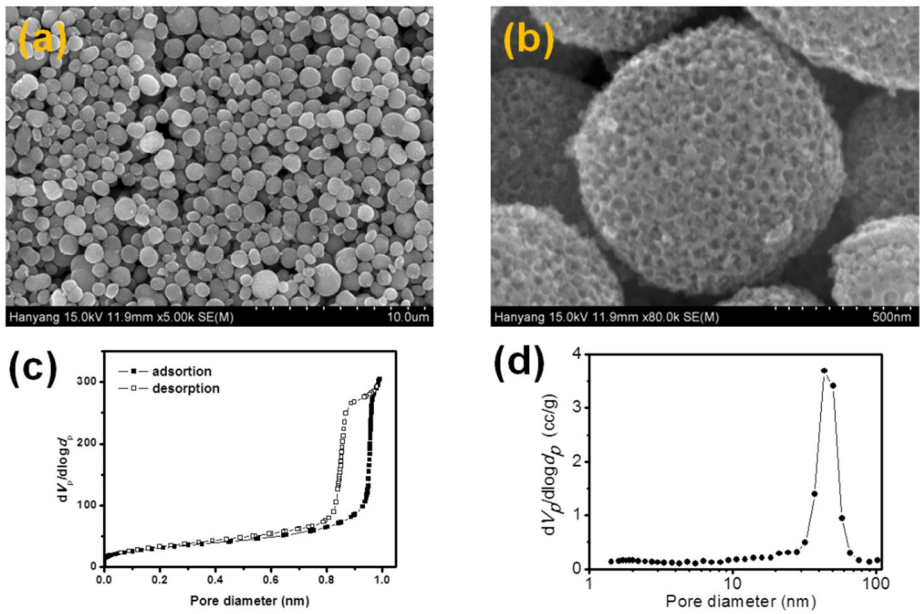

Figure 2.8. Information about '3DOm_44nm_1000nm'; (a) SEM shows that average particle size is approximately 1000nm, and (b) high magnitude SEM image shows regular pores in particles. (c) Nitrogen sorption isotherm and (d) pore distribution analyzed by BJH method show that their maximum peak position is at 44 nm.

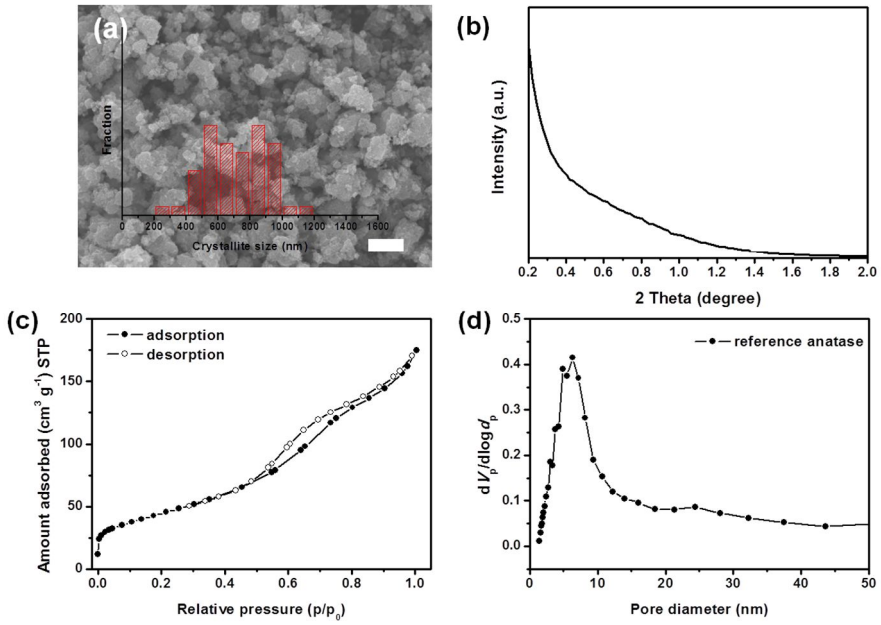

Figure 2.9. Information about 'Random_<10nm_700nm' (commercial anatase); (a) SEM shows that average particle size is approximately 700nm, and (b) SAXS reveals that there is no regularity in the sample. (c) Nitrogen sorption isotherm and (d) pore distribution analyzed by BJH method show that there is broad pore distribution under 10 nm size, and BET surface area is also comparable to that of 3DOm samples.

Table 2.1. The physical parameters of the samples; the particle size, pore diameter, crystallite size, BET surface area, total pore volume, and porosity

Sample	Particle size [a] [nm]	Pore diameter [b] [nm]	Crystallite Size [c] [nm]	S_{BET} [d] [$m^2 g^{-1}$]	V_{tot} [d] [$cm^3 g^{-1}$]
3DOm_14nm_430nm	433 (±111)	14.0	7.5	224	0.70
3DOm_14nm_1000nm	970 (± 265)	14.0	7.4	223	0.58
3DOm_24nm_580nm	585 (± 148)	24.4	8.2	171	0.75
3DOm_24nm_1000nm	985 (± 190)	24.4	8.3	190	0.65
3DOm_44nm_1000nm	1054 (± 186)	43.6	12	115	0.94
Random_<10nm_700nm	707 (± 194)	< 10	12	162	0.26

[a] Average particle sizes and its deviations are measured with 'image J' program, counted more than 50 particles.

[b], [d] Total pore volumes are measured from nitrogen sorption isotherm and pore diameters are calculated by its BJH analysis.

[c] Crystallite sizes are calculated by scherrer equation using peak at 25.3° with K factor = 0.9

2.3.2. Electrochemical performance

The influence of pore size, particle size and pore periodicity on electrochemical performance was observed through galvanostatic charge/discharge tests using electrolytes containing different Li salt concentrations. To compare the electrochemical performance between samples, a basic understanding of the reactions that occur between anatase titania and Li is required. The electrochemical reactions that occur between anatase and Li can be divided into two distinct regions in the discharge profile curves. The flat region around 1.9 V is due to Li intercalating into the bulk of anatase while the sloping region below 1.9 V is due to Li reacting at the surface of anatase. [41-43] The intercalation of Li into the bulk of anatase occurs through a two phase reaction, as evidenced by a flat plateau in the discharge profile.[41] The sloping region is composed of two electrochemical reactions; Li intercalation into the surface of anatase and pseudocapacitive reaction at surface of anatase.[42,43] The thermodynamic reaction voltage for Li intercalation into the surface of anatase is 1.9 V, which is the same as Li intercalation into the bulk of anatase. Curvature can affect the chemical potential, however, which in turn can cause the reaction voltage to vary, resulting in a curved and sloping voltage profile thereof.[44,45] The pseudocapacitive reaction is similar to the reaction that

occurs in pseudocapacitor materials, such as MnO_2, and the capacity within the sloping region is proportional to the surface area.[46] In general, nanomaterials have a high curvature and a high surface-area-to-bulk ratio that usually results in a short plateau, and a long and gradual sloping region.[47]

In the case of conventionally used 1 M electrolyte condition, the length of plateau at 1.9 V that represents bulk intercalation differs depending on the samples in Figure 2.10; the length of plateau for Random_<10nm_700nm and 3DOm_44nm_1000nm is slightly longer than that for other samples. Although the crystallite sizes of the commercial anatase and 3DOm_44nm_1000nm was similar to that of other samples, the slightly larger crystallite size of the Random_<10nm_700nm and 3DOm_44nm_1000nm (12 vs. 8 nm) may have led to this variation. Correspondingly, a larger crystallite size would show a longer plateau and a shorter sloping region. Despite the differences in the length of the plateaus, all the samples showed similar slopes and capacities below 1.9 V. Theoretically, the capacity of the sloping region should be proportional to the electrochemically active surface area and the amount of Li reacted at the surface. If theory holds true, the slopes should gradually become steeper in the sequence of 3DOm_14nm_series, 3DOm_24nm_series, Random_<10nm_780nm, and 3DOm_44nm_1000nm

based on the BET surface area. However, the experimental results did not follow this pattern. Instead, the experimental data shows that the surface area differences between samples have insignificant effect on the capacities in the sloping region. Bu and coworkers also reported similar capacities and slopes in sloping region, even though one of the samples had a surface area 1.4 times larger than the other.[48] Such results may be due to insignificant difference of BET surface area between samples, resulting in negligible changes in slopes. And, when the electrochemical performance of nonporous titania was compared with other samples, it had relatively short plateau due to small contacting area between electrolyte and active materials. It reveals that pores enhance contacting area between active materials and electrolyte, which increases the rate for the electrochemical performance happens. Furthermore, it supports that other 3DOm samples used its pores in the electrochemical reactions.

Similar results are shown in Figure 2.11, where despite the differences in discharge profiles of samples, there is a minor difference in capacities with 1 M electrolyte. The discharge profiles of all the samples (Figure 2.10) show a plateau at relatively the same location. If size and periodicity of the pore had a meaningful effect on the resistance related to Li ion diffusion through the pores, differences in *iR* drop between the samples should exist, causing the

plateau occurring at different voltages. Furthermore, the capacity ratio along the current densities shows similar behavior between samples, meaning that the aforementioned parameters did not cause any meaningful differences on the electrochemical performance at these given conditions. (Figure 2.11(b)) These findings indicate that although many reports argue that the ordered mesoporous materials more facilitate Li ion diffusion in electrolyte compared to conventional mesoporous material, such effect is generally negligible in 1 M electrolyte condition.[49, 50] On the other hand, the effect of pores in the active materials on the electrochemical performances are confirmed.

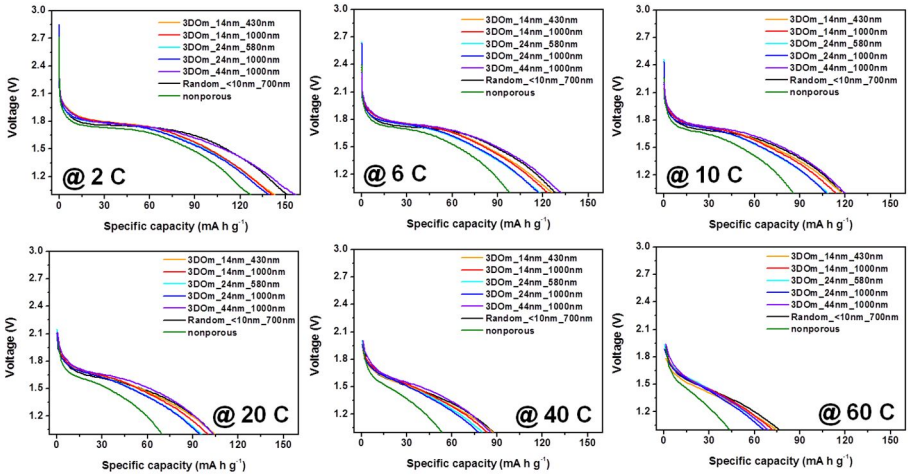

Figure 2.10. Charge/discharge profiles of the samples at 1 M electrolyte with various current densities. (1 C = 167.5 mA g^{-1})

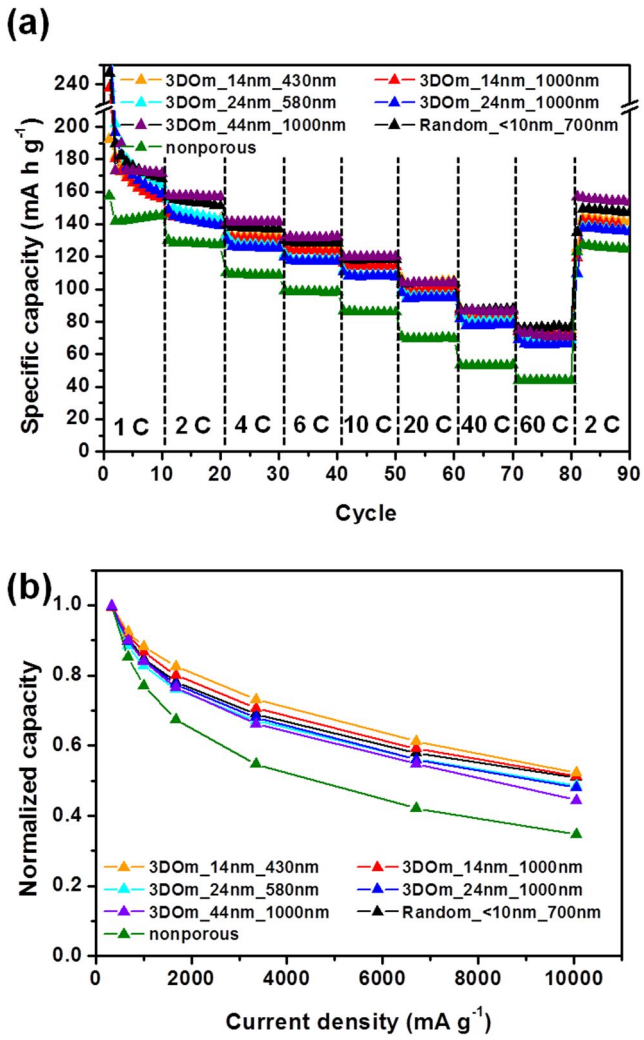

Figure 2.11. (a) Power performances and (b) normalized capacity profiles of the samples along various current densities with 1 M concentration electrolyte.

In the experiments using a salt concentration of 1 M, the samples did not show any issues related to the Li ion diffusion along the pore parameters. This implies that the concentration of Li ion was high enough to negate any problems related to the Li ion diffusion. Therefore, it was suggested that a lower concentration electrolyte (0.1 M) was implemented in order to observe what may affect Li ion depletion. As expected, the use of 0.1 M electrolyte led to different capacity ratio behaviors along the current densities At first, the effect of pore size was considered with 3DOm series with different pore sizes and almost same particle size, 1000 nm. (Figure 2.12) All samples showed similar electrochemical behavior until the current density reached 6 C. When current density exceeded 6 C, however, sudden capacity decrease was observed. In addition, 3DOm samples with pore size of 14nm and 24 nm showed similar capacity behavior along the whole current densities, but 3DOm sample with pore size of 44nm showed much enhanced electrochemical performance than that of others. It reflects that pore size in the active materials affect the electrochemical performance, which is in contrast with the case in 1 M concentration electrolyte; If the size of pore window between mesopores, where the original silica particles are contacted each other, is usually less than one third of the pore size, the pore window of 3DOm_14nm, 3DOm_24nm, and 3DOm_44nm samples were found to be

around 5 nm, 8 nm, and 15 nm, respectively. The electrochemical performances for 3DOm_14nm and 3DOm_24nm are not affected within this variation, but when the window size more increases, this effect starts to be effective.

And, the effect of particle size was also studied with same pore size and different particle sizes. (Figure 2.13) Regardless of pore size, 14 nm and 24 nm, 3DOm with larger particle size showed more rapid capacity decrease along the current densities. It means that the size of particle size affects to the electrochemical performance in 0.1 M concentration electrolyte. To further understand the reasons why the samples showed such a sudden capacity decrease, discharge profiles of 3DOm_14nm samples in 0.1 M and 1 M electrolyte were compared. (Figure 2.14) As Figure 2.14 shows, the plateau seen at 1 M electrolyte shifts to a lower potential in 0.1 M electrolyte, which can be explained by an increase in overpotential. The increase in *iR* drop most likely originates from a decrease in salt concentration.[51, 52] The slope after the plateau, however, shows a similar gradient in 1 M and 0.1 M electrolyte. From this observation, it can be hypothesized that there is no differences between the reactions at the surface in both electrolytes. This result implies that Li ion depletion does not occur inside the particles at these conditions. In the case of 3DOm_14nm_430nm, these trends continue up

to a 20 C rate, and similar capacities are in both electrolytes. However, significant differences are observed at a rate of 40 C. The most noticeable differences were the shortening of the length of the plateau and the near disappearance of the sloping region. The shortened plateau signifies a smaller portion of the bulk being utilized for intercalation than usual, and the near disappearance of the slope signifies the absence of surface reactions. These phenomena seem to originate from the depletion of Li ion inside the mesopores in particle. It reflects that the diffusion of the Li ion through the mesopores in particle does not occur fast enough to allow the electrochemical reaction to occur at a steady and continuous rate. This generates a dead volume of the active materials, which leads the active materials with smaller capacities and different discharge profiles. When this principle is applied to the cases considered above, it reflects that the Li ion depletion could take place more easily in larger particles than smaller particles. In addition, large mesopores in the active materials also facilitate the Li ion diffusion through the electrolyte in mesopores, and what really affects to the Li ion diffusion is not a pore size, but a window size in our case, 3DOm structure.

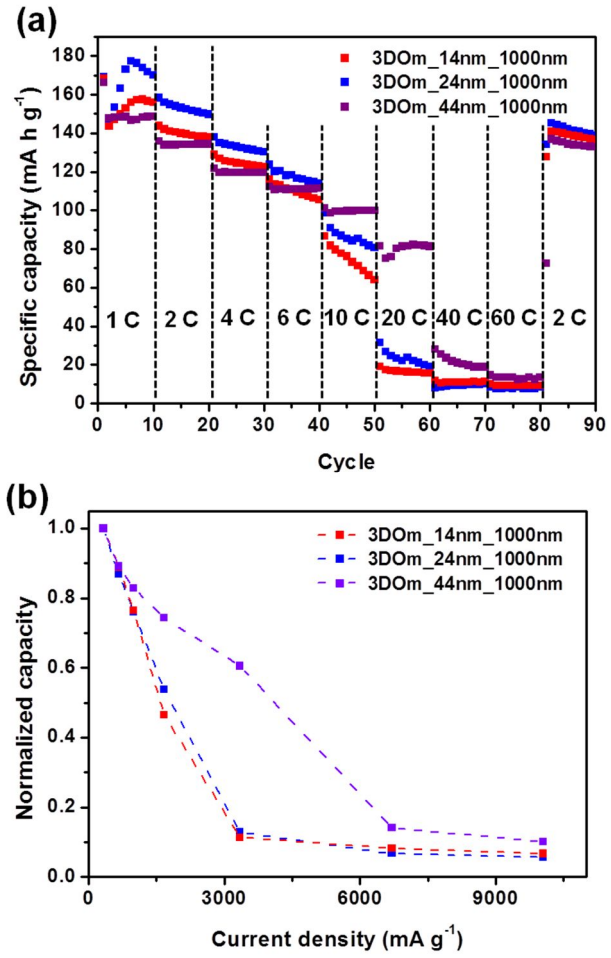

Figure 2.12. (a) Power performance and (b) normalized capacity profile of 3DOm samples with different pore size and almost same particle size at 0.1 M concentration electrolyte

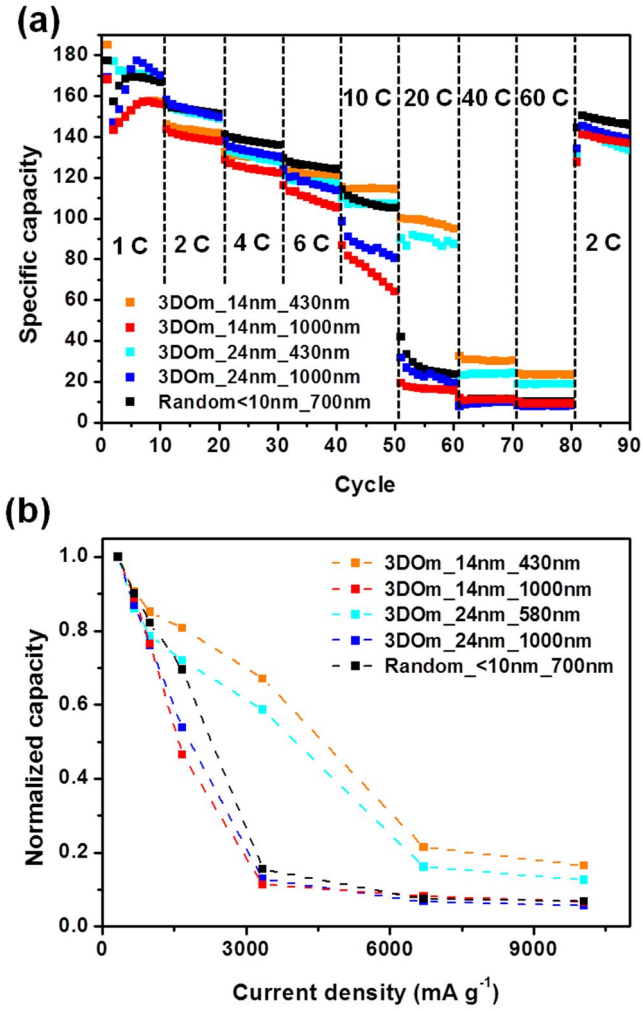

Figure 2.13. (a) Power performance and (b) normalized capacity profile of 3DOm samples with different particle sizes and commercial anatase at 0.1 M concentration electrolyte

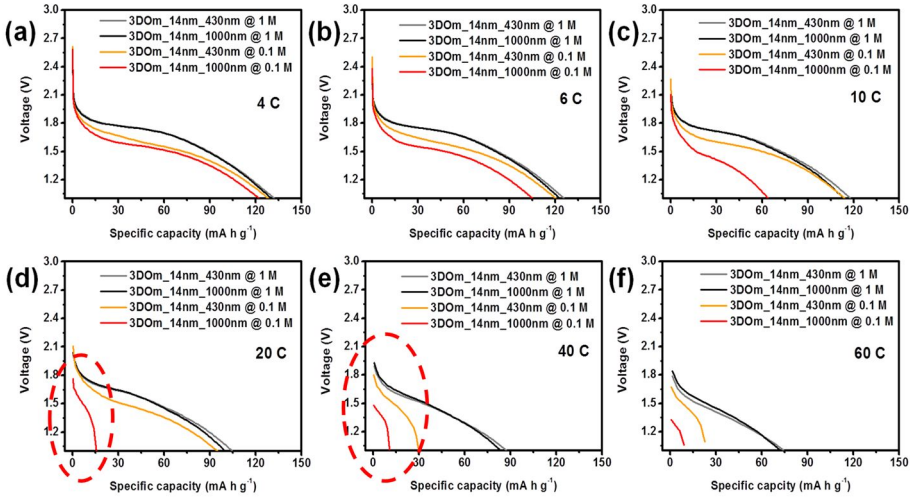

Figure 2.14. Discharge profiles of 3DOm_14nm_430nm and 3DOm_14nm _1000nm with 1 M and 0.1 M concentration of electrolyte at (a) 4 C, (b) 6 C, (c) 10 C, (d) 20 C, (e) 40 C, and (f) 60 C. (1 C = 167.5 mA g^{-1})

2.3.3. Mathematical approach using Thiele modulus

To describe the experimental results above, the mathematical model which is usually used in porous catalyst system is introduced. [53] Let's think of porous spherical material with radius of R. The sign of flux is assumed to have positive value when the direction of flux is outward direction, which is direction of increasing r, and it makes the direction of diffusion be negative, because of its inward direction of diffusion. When we think of the mole balance over the shell thickness Δr of porous spherical material, and assume equilibrium within that volume,

$$(\text{In at } r) - (\text{out at } r + \Delta r) + (\text{Generation within } \Delta r) = 0$$

$$\left(W_{Li,r} \cdot 4\pi r^2|_r\right) - \left(W_{Li,r} \cdot 4\pi r^2|_{r+\Delta r}\right) + \left(r_{Li} \cdot \rho_c \cdot 4\pi r_m{}^2 \, \Delta r \cdot (1-\varphi_p)\right) = 0$$

where $W_{Li,r}$ is diffusion flux of Li salt, r is radius, r_{Li} is a rate of reaction, ρ_c is density of material, and r_m is mean radius of the volume of shell thickness Δr. When we develop the equations above,

$$\frac{d(W_{Li,r}\, r^2)}{dr} - r_{Li}\, \rho_c\, r^2 (1-\varphi_p) = 0$$

$$W_{Li,r} = -D_e' \frac{dC_{Li}}{dr}$$

The lithiation reaction consumes Li salts with proportional to current density. When the rate of lithiation is assumed to have same value along the

radius, when normalized by mass of active materials, then, r_{Li} can have

$$r_{Li} = -\frac{j}{96485}\left[\frac{mol}{sec\cdot g}\right], \qquad j = \text{current density } [=]\ \frac{A}{g}$$

$$\frac{d[-D_e\left(\frac{dC_{Li}}{dr}\right)r^2]}{dr} + \frac{j\cdot\rho_c}{96485}\, r^2(1-\varphi_p) = 0, \quad \frac{j\cdot\rho_c}{96485} = k_0$$

$$-D_e' r^2 \frac{d^2C_{Li}}{dr^2} - 2D_e' r \frac{dC_{Li}}{dr} + \frac{j\cdot\rho_c\cdot(1-\varphi_p)}{F} r^2 = 0$$

$$\frac{d^2C_{Li}}{dr^2} + \frac{2}{r}\frac{dC_{Li}}{dr} - \frac{j\cdot\rho_c\cdot(1-\varphi_p)}{F\cdot D_e'} = 0$$

When $\frac{D_e'}{(1-\varphi_p)}$ term is compressed to D_e, the system diffusion co

efficient, which includes all the structural information of mesopores,

equation is,

$$\frac{d^2C_{Li}}{dr^2} + \frac{2}{r}\frac{dC_{Li}}{dr} - \frac{j\cdot\rho_c}{F\cdot D_e} = 0$$

When we use dimensionless forms of concentration and radius,

$$\Psi = \frac{C_{Li}}{C_{Li,s}}, \quad \lambda = \frac{r}{R}$$

$$\frac{dC_{Li}}{dr} = \frac{d\Psi}{d\lambda}\left(\frac{dC_{Li}}{dr}\right)\frac{d\lambda}{dr} = \frac{C_{Li,s}}{R}\left(\frac{d\Psi}{d\lambda}\right)$$

$$\frac{d^2C_{Li}}{dr^2} = \frac{d^2\Psi}{d\lambda^2}\frac{d\lambda}{dr}\frac{C_{Li,s}}{R} = \frac{C_{Li,s}}{R}\left(\frac{d^2\Psi}{d\lambda^2}\right)$$

where R is radius of porous spherical material, D_e is effective diffusion coefficient ($D_e = \frac{D_{AB}\,\varphi_p\,\sigma_c}{\tilde{\tau}}$), and $C_{Li,s}$ is the concentration of Li salt at r = R,

which is assumed to be same with the concentration of used electrolyte. (1 M or 0.1 M) When two equations are introduced into the equation above,

$$\frac{d^2\Psi}{d\lambda^2} + \frac{2}{\lambda}\frac{d\Psi}{d\lambda} - \frac{k_0 R^2}{D_e C_{Li,s}} = 0$$

Last term in left part of the equation above is determined by experimental conditions, and it can be compressed to $\phi_0{}^2$, where ϕ_0 is 'thiele modulus'.

$$\phi_0{}^2 = \frac{k_0 R^2}{D_e C_{Li,s}} = \frac{j \cdot \rho_c}{96485}\frac{R^2}{D_e C_{Li,s}}$$

$$\frac{d^2\Psi}{d\lambda^2} + \frac{2}{\lambda}\frac{d\Psi}{d\lambda} - \phi_0{}^2 = 0$$

Using boundary conditions,

$$\text{B.C.s: } \Psi \text{ is finete } @\ \lambda = 0,\ \Psi = 1\ @\ \lambda = 1,\ \frac{d\Psi}{d\lambda} = 0\ @\ \lambda = 0$$

Solve equation, and the final solution is

$$\therefore\ \Psi = \frac{1}{6}\phi_0{}^2\lambda^2 + 1 - \frac{1}{6}\phi_0{}^2$$

According to the model described above, the main parameter which determines the profile of Li ion concentration inside of particle is "thiele modulus". The thiele modulus is proportional to the particle size and inversely proportional to root of the effective diffusion coefficient. Large particle size means long diffusion path in the electrolyte, therefore, Li ion diffusion becomes more important for large particles than small particles. In addition, pore size or window size could affect to diffusion coefficient. This

can explain the phenomena that Li ion depletion is more sensitively depend on particle size, rather than pore size and pore structure. Using the model, the Li ion concentration profiles can be expected along the values of ϕ_0^2, and it is depicted in Figure 2.15. When the ϕ_0^2 has small value, there is no Li ion depletion inside of the particle. But, when ϕ_0^2 increases, Li ions start to be depleted from the core part of the particle. Thiele modulus can be calculated from the experimental values, thus thiele modulus at 1000 nm, 40 C, and 0.1 M, where Li ion depletion happens are calculated. If the diffusion coefficient is assumed to have 10^{-6} cm^2 sec order, which is ordinary value in liquid electrolyte, thiele modulus have 10^{-3} order. In this range, Li ion depletion cannot be explained. When the diffusion coefficient is assumed to have 10^{-10} cm^2 sec order, on the other hand, thiele modulus is around 60, and it can explain Li ion depletion in the active material. Furthermore, it is found that when the effective diffusion coefficient is assumed to be around $2x10^{-10}$ cm^2 sec^{-1}, the model fits into the experiment well. It reflects that Li ion diffusion in the electrolyte within mesopores can be slower than that in bulk electrolyte. Diffusion in nano-sized pores is more affected from shear stress at the wall, and window size affects to jumping rate. In addition, there are many reports that propose diffusion coefficient with 10^{-10} cm^2 sec^{-1} order.[54-58]

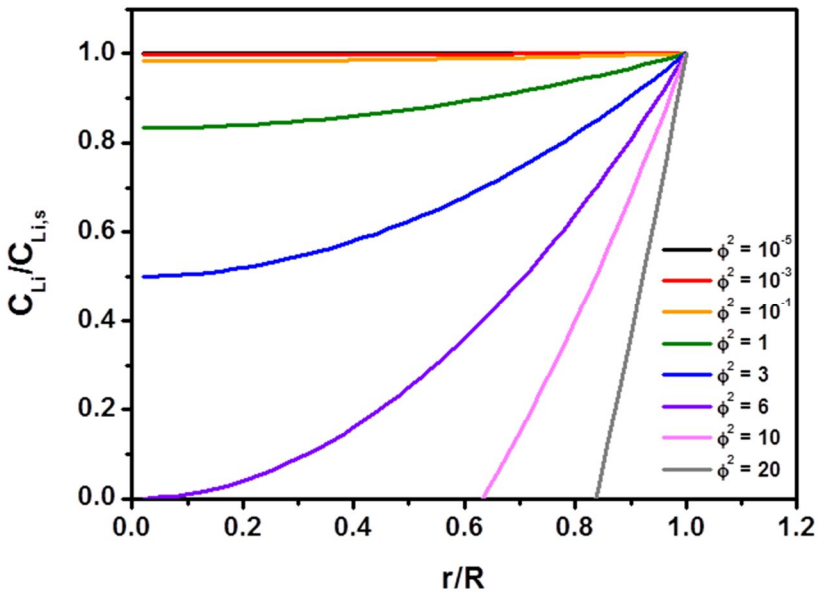

Figure 2.15. Calculated concentration profiles along various square of thiele modulus.

Based on this result, the critical size of particle that starts to show Li ion depletion along the various current densities are calculated and depicted in Figure 2.16. (The criterion is assumed to be $\phi_0{}^2 = 6$) When the particle is less than 1 μm, Li ion depletion does not happen even around 10 A g^{-1}. Therefore, it is hard to think that the improvement of the diffusion can enhance the electrochemical performance in this case. As the current densities increases, however, the critical size dramatically decreases. Therefore, Li ion diffusion should also be considered in the case of large particles.

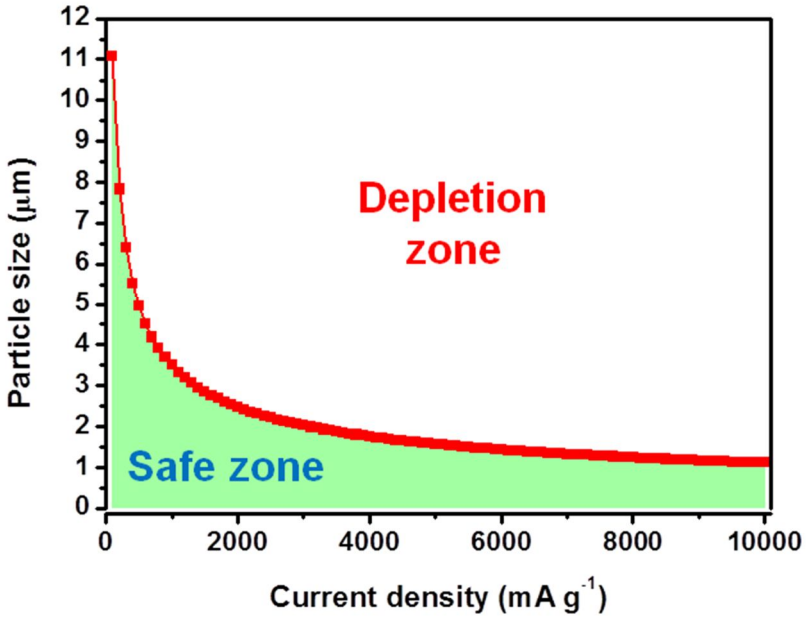

Figure 2.16. Calculated boundaries where salt depletion starts to show.

2.4. Conclusion

In this study, 3DOm titania particles with different pore sizes and particle sizes were synthesized by a nanocasting method using a size tunable close-packed silica particle. Using the structurally well-defined 3DOm titania particles and commercial titania particle with a random mesopore, it was examined that how these pore parameters affected the electrochemical performance along with different concentrations of Li ion. In the experiments using 1 M electrolyte, it is confirmed that the mesopores in active material can improve the electrochemical performance due to enlarged contacting area between active material and electrolyte. Except nonporous titania, however, all the samples showed a similar electrochemical behavior regardless of the pore size, particle size and periodicity along the applied current densities. On the other hand, in the experiments using 0.1 M electrolyte, the samples with large particle sizes and small pore sizes started to show Li ion depletion at lower current densities. From these results, it can be concluded that although many reports argue that ordered mesoporous materials facilitate the Li ion diffusion in electrolyte compared to a conventional mesoporous material, such effect is negligible in 1 M electrolyte under our experimental condition. It is also confirmed that sizes of mesoporous material and pore size are influential parameter for Li ion

diffusion through mesoporous material, but their effect is negligible in 1 M electrolyte.

In order to rationalize the experimental results, a mathematical model that contains the Thiele modulus parameters, frequently used in heterogeneous catalyst systems was adopted in our system. In addition, critical sizes that start to show the Li ion depletion along the various current densities are calculated using this model. According to the calculation, the Li ion depletion is hardly seen under a particle size of 1 μm in 1 M electrolyte, which is also experimentally observed. These results will be helpful in understanding Li ion diffusion through mesopores in mesoporous materials, so that the Li ion depletion problems can be negated and optimal performance could be achieved at ideal current densities.

Chapter 3. Reaction mechanism and kinetics in Li-Si system

3.1. Introduction

3.1.1. General information on Si

Si is one of the Li-alloy materials. Li-alloy materials had attracted many attentions as a substitute for Li metal in the specific secondary batteries with molten salt electrolyte, which work at higher temperature than melt temperature of Li metal, 400~450 °C. The representative example is Li-alloy/FeS_2 cell with molten chloride salt electrolyte. [59] At this high temperature, Li and Si react with two-phase reaction forming crystalline Li_xSi ($0 \leq x \leq 4.4$) at several flat voltage regions. In room temperature, however, there is not enough energy to overcome the energy barrier for crystallization. Therefore, the reactions proceed within amorphous phase of Si (*a*-Li_xSi), rather than forming crystalline phase, and then only Si can be crystallized at low potential, which has enough energy. (Final product is assumed to be *c*-$Li_{3.75}Si$ under 50 mV) This information is well introduced in the research fields, and it is also possible to understand in thermodynamic aspect using Gibbs free energy curve (Figure 3.1) [60, 61] According to J.

Dahn group, the reaction between Li and Si can be categorized into two groups, and the criteria is local environment of Li along the lithiation proceeds. [62]

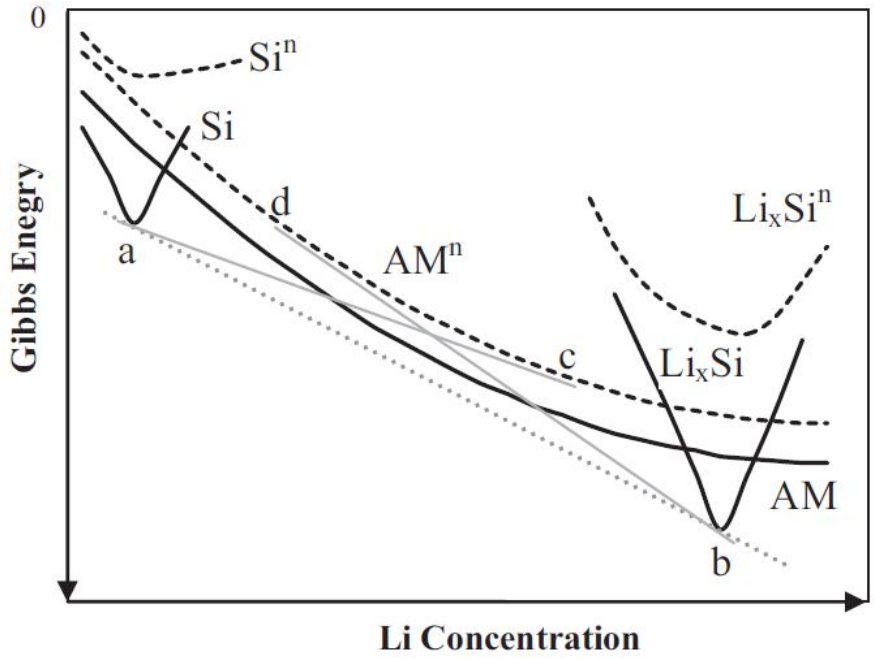

Figure 3.1. Gibbs free energy diagram of the reaction between Li and Si. (Adapted from the W.-J Zhang, J. Power Sources, **2011**, 196, 877)

As Si is introduced as one of the anode materials for LIBs in part 1, Si suffers from large volume expansion over 300 % along the reaction with Li, which result in electric disconnection between active materials and current collector. This kind of problems related to volume expansion cannot be avoided for the materials with large specific capacities, such as iron oxide, tin oxide, and tin, due to intrinsic volume of Li itself. [63, 64] In addition, Si has intrinsically low electric conductivity around 10^{-3} S cm. To solve such problems, Si is made into nano-structure, which can effectively relieve stresses originating from volume expansion, resulting in alleviating pulverization. And, coating with conductive materials, such as carbon, is another method. These kinds of approaches have been tried actively by many research groups. On the other hand, there is lack of thermodynamic and kinetic understanding about Li-Si system. For example, the reaction between Li and Si had been assumed to be proceed with solid-solution reaction due to its sloping lithiation/delithiation profiles. Lately, however, two papers which propose lithiation of Si is proceed with two-phase reaction using *in-situ* and *ex-situ* TEM method. This ambiguity about the reaction between Li and Si comes from amorphization of Si along the lithiation; amorphous structure of Si is hard to analyze using routine tools, such as TEM, and XRD.

3.1.2. Scheme of this study

In this study, the reaction mechanism between Li and Si is confirmed. Open-circuit voltages (OCV) are observed along various temperature and depth of lithiation using commercial nano-Si powders, and thermodynamic parameters, such as $\Delta S, \Delta H$ are calculated using the information acquired above. These thermodynamic parameters can help to figure out whether the reaction between Li and Si proceeds with solid-solution reaction or two-phase reaction.

Furthermore, the kinetic studies are carried out using various current densities. The responses of two reaction regions along various current densities are deconvoluted and confirmed. The reasons for these phenomena are revealed with electrochemical methods, such as electrochemical impedance spectroscopy (EIS), galvanostatic intermittent titration technique (GITT).

Through these findings, deep understanding of reaction mechanism of Li-Si system is achieved. And, the strategies to improve electrochemical performance of Si or the idea about which part should be modified are discussed.

3.2. Experimental section

The slurry which is composed of 60 wt.% of commercial nano-Si from alfa aesar, 20 wt.% of conducting agent (Super-p), and 20 wt.% of polyamideimide (PAI) binder was mixed with *N*-methyl-2-pyrrolidone solvent, and spread onto a copper foil using Dr. blade method. The morphology and phase are confirmed with SEM and XRD. (Figure 3.2) To activate the PAI binder, the as-prepared electrode was heat-treated at 350 °C under Ar atmosphere for 90 min, then vacuum-dried at 120 °C for 8 h. The prepared electrodes were transferred to an Ar-filled glove box, and cells were assembled. The electrolyte was 1.5 M LiPF6 ethylene carbonate (EC) / diethyl carbonate (DEC) / fluoroethylene carbonate (FEC) (5/70/25 vol., Panatech, Korea), and the separator was from SK innovation. Li metal was used as a counter electrode, and the cell type was 2016.

Before conducting thermodynamic study, pre-cycle was proceed; at first cycle, lithiation was done in a current density of 200 mA g^{-1} to 0.01 V following a constant voltage of 0.01 V, until the current density had reached 40 mA g^{-1}, and delithiation was done in a current density of 200 mA g^{-1} to 1.5 V; through this process, whole Si in the electrode is assume to be used. From second cycle, lithiation was done in a current density of 400 mA g^{-1} to 0.06 V, and delithiation was done in a current density of 400 mA g^{-1} to 1.5 V;

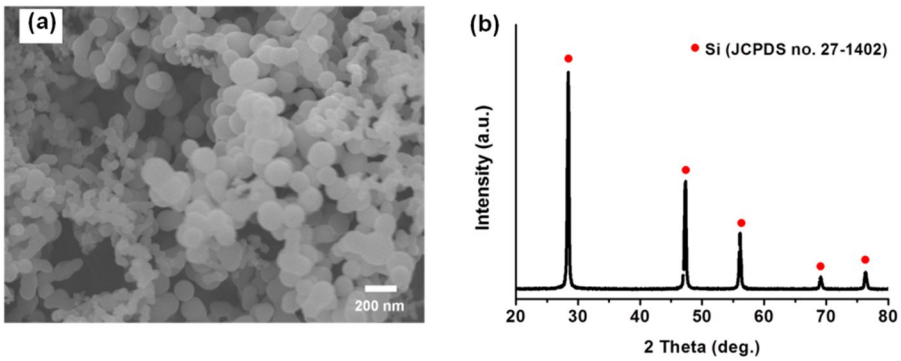

Figure 3.2. (a) SEM and (b) XRD of commercial nano-Si.

according to J. Dahn group, *a*-Li_xSi is crystallized to *c*-Li_xSi under 50 mV. [66] When LixSi is crystallized, delithiation profile is different from delithiation profile of *a*-Li_xSi. To avoid crystallization of *a*-Li_xSi, therefore, cut-off voltage is determined to 60 mV. Before thermodynamic study, three cycles were conducted to make whole Si to amorphous phase, which is exact reacting phase, and targeted voltages were fixed over 12 h to make equilibrium states. The cells after pre-cycles were transferred to oven, and make them be equilibrium at several temperatures, 25, 30, 35, 40, 45, 50 °C for 30 min, and resulting OCVs were recorded.

To study kinetic properties of Li-Si system, first cycle was conducted just same with the method mentioned above. After first formation cycle, rate performance was carried out with various current densities, 400, 800, 1600, 2400, 3200 mA g^{-1}, and second lithiation/delithiation profiles of each rates were analyzed using differential capacity profiles. To avoid or minimize cell degradation due to repeated volume change of Si, each stage was conducted for just three cycles.

To measure EIS, a symmetric cell was used to separate the effects from the Li metal side; two cells, which were cycled to the same condition, 0.25 V, and 0.08 V in lithiation, and 0.30 V, and 0.50 V in delithiation, were transferred into an Ar-filled glove box, disassembled, and re-assembled into

a symmetric cells. EIS was conducted with OCV in 10 mV amplitude, and the frequency range was from 100 kHz to 50 mHz (Zahner, Germany).

GITT method was carried out with 100 mA g^{-1} for 10 min and rest for 20 min.

3.3. Results and discussion

3.3.1 Reaction mechanism of Li-Si system

As introduced in part 1, open-circuit voltage of LIBs is determined by the Gibbs free energy, ΔG of the net reaction, which means the amount of maximum work that can be done. Several thermodynamic parameters, such as ΔS, and ΔH, can be obtained from the temperature dependence of the open-circuit voltage using thermodynamic relations described below. [67]

$$\Delta G = \Delta H - T\Delta S = \Delta U + P\Delta V - T\Delta S = -nFE$$

where ΔH is enthalpy change, T is temperature, ΔS is entropy change, P is pressure, ΔV volume change, n is number of electrons involved in the reaction, F is faradaic constant, and E is voltage. Assume $dP = 0$, and replacing molar fraction by composition $x = n/N_A$

$$\left.\frac{\partial S}{\partial x}\right|_T = F \left.\frac{\partial E}{\partial T}\right|_x$$

and

$$\left.\frac{\partial H}{\partial x}\right|_T = -FE + T \left.\frac{\partial S}{\partial x}\right|_T = -FE + TF \left.\frac{\partial E}{\partial T}\right|_x$$

(Detailed derivation is as follows:

$$-F\left.\frac{\partial E_0}{\partial T}\right|_{x,p} = \left.\frac{\partial \Delta H}{\partial T}\right|_{x,p} - T\left.\frac{\partial \Delta S}{\partial T}\right|_{x,p} - \Delta S$$

$$\left.\frac{\partial \Delta H}{\partial T}\right|_{x,p} = \Delta \mathrm{C_p(T)} \quad \text{and} \quad \left.\frac{\partial \Delta S}{\partial T}\right|_{x,p} = \frac{\Delta \mathrm{C_p(T)}}{\mathrm{T}}$$

$$C_p = 1943 \left(\frac{T}{\Theta_D}\right)^3 + \frac{\alpha^2 VT}{\kappa_T}$$

where Θ_D is debye temperature ($\Theta_{D,\mathrm{Si}} = 645$ K), α is thermal expansion coefficient, and κ_T is isothermal compressibility.

$$-F\frac{\partial E_0}{\partial T}\Big|_{x,p} = \Delta \mathrm{C_p(T)} - T\frac{\Delta \mathrm{C_p(T)}}{\mathrm{T}} - \Delta S = -\Delta S = -\frac{\partial S}{\partial x}\Big|_T \quad)$$

In the relations above, dS and dH means the change in entropy and enthalpy that occur when an amount of Li, dx is inserted into the active material. The reference for dS and dH is the bcc Li metal plus the active materials with composition of $(x - dx)$. From the relations, it can be found that the slope of open-circuit voltages along temperatures is directly related to the entropy changes along the change of mole fraction of Li. Some research groups had used these thermodynamic relations to obtain detailed properties related to the reaction processes.[68-70]

The information about entropy changes gives some clues about whether the reaction proceeds with solid-solution reaction or two-phase reaction; if the reaction proceeds with two-phase reaction, entropy change should be constant. It is due to the fact that same reactions are conducted along the process proceeds, which is same principle with the phenomena that shows flat voltage plateau in two-phase reactions. There is no compositional change in each component, but is phase boundary shift, resulted from the change in

total amount of Li. On the other hand, if the reaction proceeds with solid-solution reaction, there is configurational entropy change as the amount of Li or vacancy varies, resulting in logarithmic relation of entropy change with composition.

$$\frac{\partial S}{\partial x} = -\mathrm{k_B}\frac{\partial}{\partial x}[x\ln x + (1-x)\ln(1-x)] = k_B \ln\frac{1-x}{x}$$

where k_B is the Boltzman constant.

In this study, Si electrodes after three cycles reached specific voltages, and made to be equilibrium state by rest them for 30 min at various temperatures. Figure 3.3 shows how OCV changes along temperatures. As temperature increases, all OCVs vary. From the equation above, it tells us that ΔS varies along the Li compositions. It is somehow obvious because bcc Li metal might have smaller entropy than *a*-Li_xSi.

$$a - \mathrm{Si} + \mathrm{x\ Li} = a - \mathrm{Li_xSi}$$

$$\Delta S = S_{a-\mathrm{Li_xSi}} - (S_{a-\mathrm{Si}} + \mathrm{x}\, S_{\mathrm{Li}}) > 0$$

Therefore, when Li contents increase, the amount of *a*-Li_xSi, which has higher entropy, increases, resulting to have positive ΔS.

In Figure 3.4, exact values of entropy changes are depicted along OCVs. Three regions can be divided depending on behavior of entropy changes, and they are labeled to region A, region B, and region C in Figure 3.4.

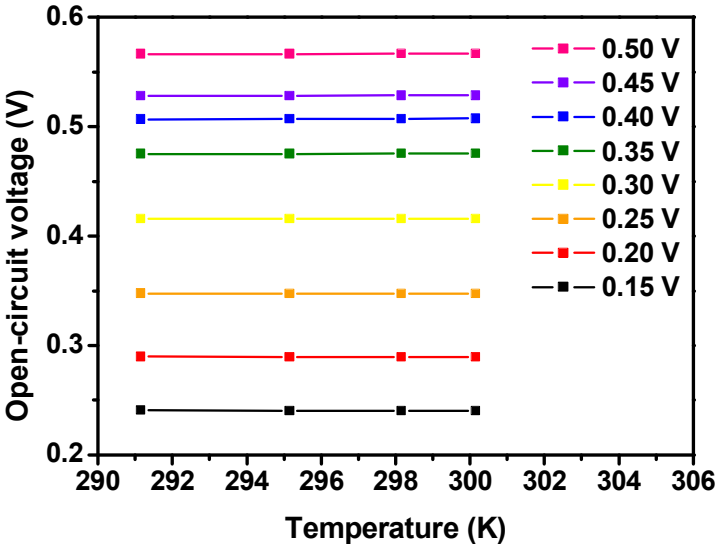

Figure 3.3. OCV changes along the temperature (OCV in the legend is OCV at 298 K)

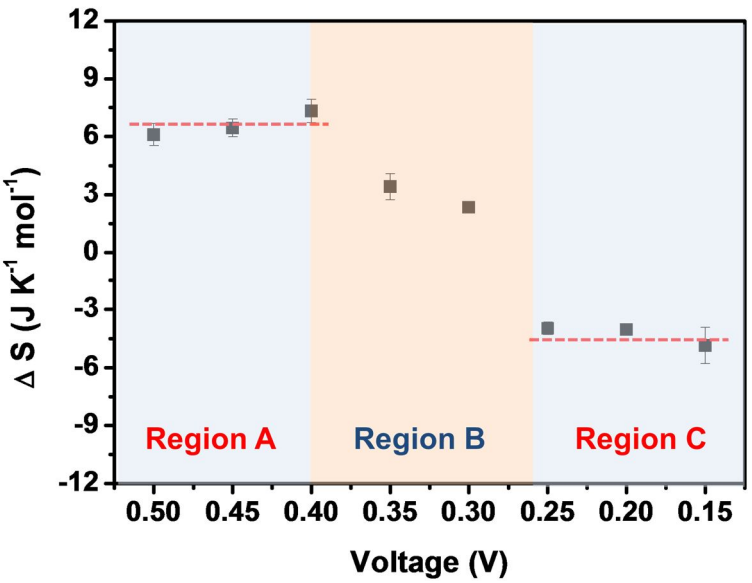

Figure 3.4. Calculated entropy changes in Li-Si system along the reaction voltages.

Region A. Constant entropy changes approximately 8 J K^{-1} mol^{-1}: According to the relation between reaction mechanism and entropy change, the reaction between Li and Si in this region seems to be two-phase reaction.

Region B. Decrease in entropy changes: As the amount of Li increases, entropy change decreases, which reflecting that the reaction in this region is solid-solution reaction.

Region C. Constant entropy changes approximately -5 J K^{-1} mol^{-1}: constant entropy change along the reaction proceeds, which means the reaction between Li and Si in this region seems to be two-phase reaction. The difference between region C and region A is the value of entropy change.

(If whole regions are considered to be conducted by solid-solution reaction, this tendency of entropy change cannot be fitted into one logarithmic equation; usually, logarithmic equation shows rapid decrease in both end of x-axis, and gentle decrease in middle of x-axis as in Figure 3.5. These behaviors are different from the behavior in Figure 3.4)

To understand the regions divided above, detailed information about how Li and Si react and how these reactions can be categorized is necessary.

According to J. Dahn, the reaction between Li and Si can be divided into two regions [72]: first region is related to the reaction where inserted Li surrounds Si. This region corresponds to first sloping region in lithiation/delithiation profile of Si, and will be name to reduction 1 (R1)/oxidation 1 (O1). The energy of the state is relatively small, i.e. high voltage region, because the repulsion between Li-Li is small. As more Li inserted into Si, Li cannot surround Si any more. Instead, inserted Li starts to surround the Li previously inserted. This region correspond to second sloping region in lithiation/delithiation profile of Si, and will be named to reduction 2 (R2)/oxidation 2 (O2). In this case, the repulsion between Li-Li increases, and the reaction conducted at higher energy, i.e. lower voltage region. These behaviors are also confirmed with solid state ^{7}Li-NMR by C.P. Grey group. [71,72] Between these two sloping regions, transition region is also observed, and the whole regions are illustrated in Figure 3.6 for better understanding.

Based on the information above, region A corresponds to R1(O1), region C corresponds to R2(O2), and region B corresponds to transition state. Therefore, it can be concluded that reaction of Li and Si is composed of two parts of two-phase reaction, and one solid-state region, which connect two

two-phase reactions. These findings are somehow different from general understanding of the reaction between Li and Si, which is solid-solution reaction.

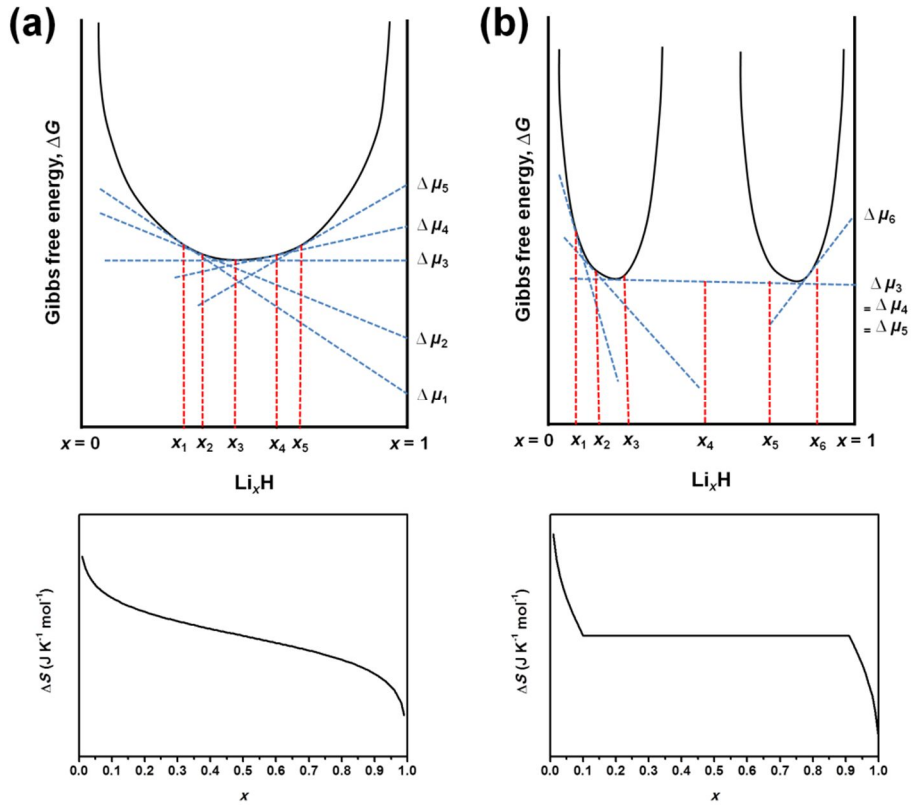

Figure 3.5. The entropy change in (a) solid-solution reaction, and (b) two-phase reaction.

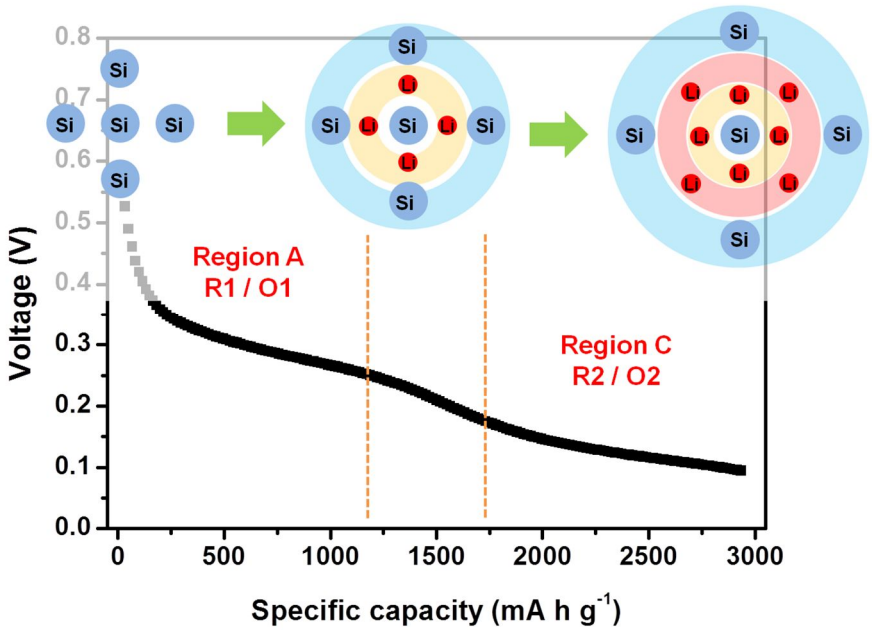

Figure 3.6. Expected reaction process along the amount of Li.

Then, why the region A shows positive entropy change, and the region C shows negative entropy change? The reaction equations adding an incremental amount of Li into the host material and corresponding entropy changes are written as follows:

$$\text{Region A:}\quad \frac{dx}{x}\ a-\text{Si}+dx\ \text{Li}=\frac{dx}{x}\ a-\text{Li}_x\text{Si}$$

$$dS_{\text{region A}}=\frac{dx}{x}\ S_{a-\text{Li}_x\text{Si}}-\left(\frac{dx}{x}\ S_{a-\text{Si}}+\ dx\ S_{\text{Li}}\right)$$

$$\text{Region C:}\quad \frac{dx}{y-x}\ a-\text{Li}_x\text{Si}+dx\ \text{Li}=\frac{dx}{y-x}\ a-\text{Li}_y\text{Si}$$

$$dS_{\text{region C}}=\frac{dx}{y-x}\ S_{a-\text{Li}_y\text{Si}}-\left(\frac{dx}{y-x}\ S_{a-\text{Li}_x\text{Si}}+\ dx\ S_{\text{Li}}\right)$$

From the entropy change in region A, it can be deduced that entropy of *a*-Li_xSi is larger than that of *a*-Si. In region C, on the other hand, the entropy of *a*-Li_ySi is smaller than that of *a*-Li_xSi, which resulting in negative entropy change

The region B seems to correspond to transition state between R1(O1) and R2(O2), and conducted by solid-solution reaction. According to logarithmic relation of entropy change for solid-solution reaction (Figure 3.5), it shows odd function behavior centered at $x = 0.5$. In Figure 3.4, however, region B only shows half of logarithmic behavior. It is easy to understand using Gibbs free energy diagram of reactions in Figure 3.7.

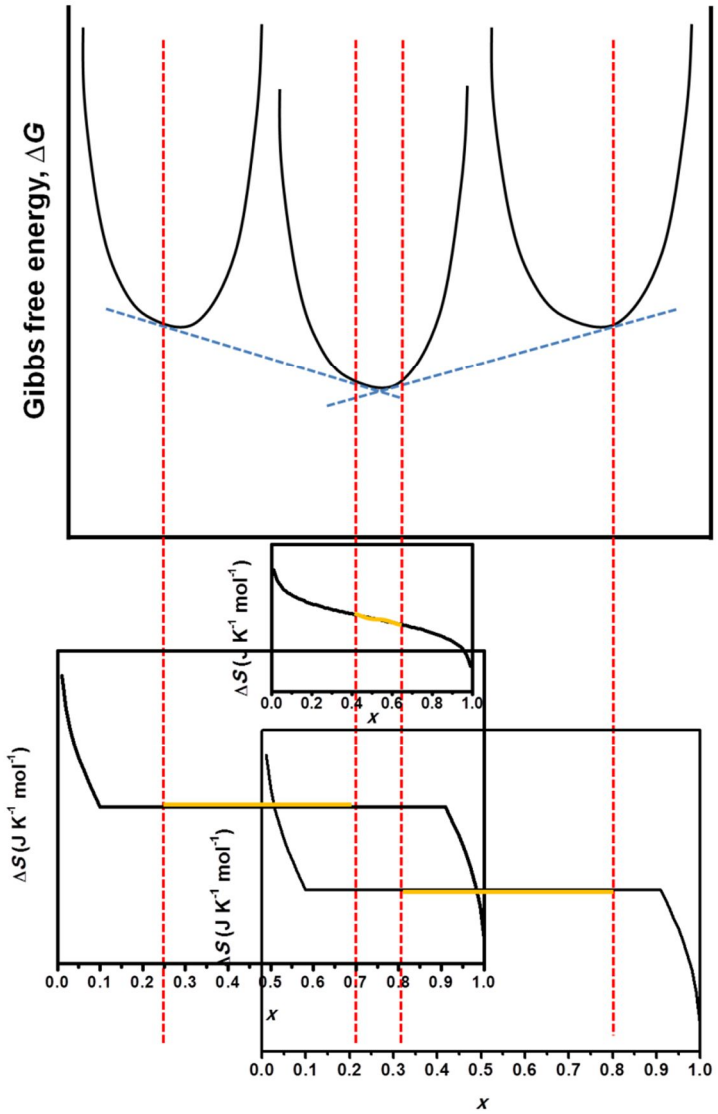

Figure 3.7. Gibbs free energy diagram of the reaction between Li and Si, and expected trend in the entropy change.

The full logarithmic relation can be completed when the reaction in whole Li fraction is conducted by solid-solution reaction. If there is two-phase reaction before or after solid-solution reaction, however, only limited region of Li fraction can be proceed by solid-solution reaction, like in Figure 3.7. Therefore, specific region around mole fraction of 0.5 can be utilized by solid-solution reaction.

There is also another evidence for insisting that the reaction between Li and Si is two-phase reaction;the profile of Li diffusion coefficient along the amount of Li. When the diffusion coefficients are measured by GITT method, [73] there are two regions where show sudden decrease and recovery, like a U-shaped curves. (Figure 3.8) According to C. Wang et al., when the diffusion coefficient of the materials with two-phase reaction is measured using traditional electrochemical method, such as EIS, potentiostatic intermittent titration technique (PITT) and GITT, there is U-shaped curve at two-phase region.[74] In two phase region, ions are transported by diffusion and phase boundary movement. Therefore, apparent diffusion coefficient measured by traditional methods can be affected by both ion diffusion, and phase boundary movement, which resulting in incorrect and lower magnitude of measured values. Moreover, there are more examples that shows 2-3 orders of magnitude lower apparent diffusion coefficient in two-

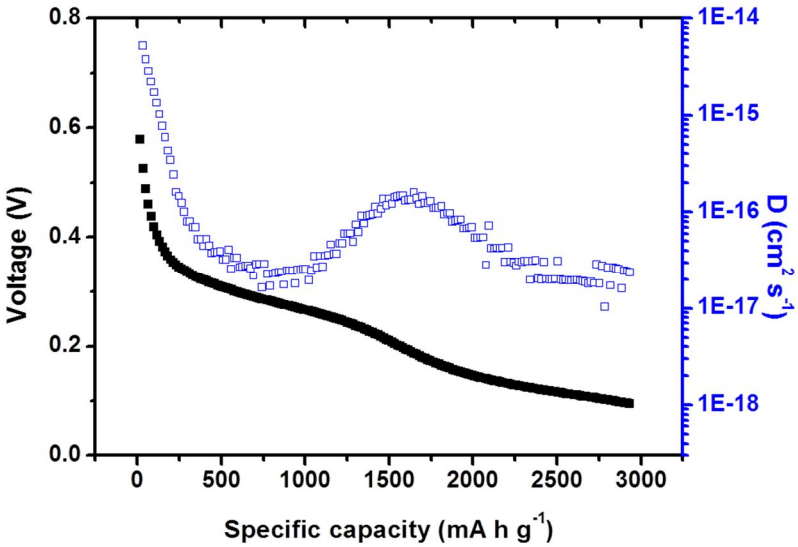

Figure 3.8. Results of GITT: diffusion coefficients and OCV along the specific capacity.

phase region than those in solid solution region.[75-77] Even the fact that Si also shows the regions that have lower orders of magnitude of diffusion coefficient than other region is somehow indirect, but, it still has logical validity. Furthermore, it is more plausible to explain the Li-Si reaction with two-phase reaction than with solid-solution reaction. Therefore, it could be concluded that the reaction between Li and Si is two-phase reaction.

Then, why the Li-Si system shows sloping lithiation/delithiatoin profile, even though it proceeds with two-phase reaction? The possible explanation is the effect from strain. Strain can affect to the chemical potential at interface between active materials and electrolyte, which can result in different voltages. As the reaction goes on, strain can be changed gradually, thus the voltage also can be changed gradually. In addition, there is another possibility that the two-phase reaction in Li-Si system is not an ordinary two-phase reaction between two phases with fixed stoichiometries. For example, the stoichiometries of two phases can be changed, resulting in changing in voltages.

3.3.2. How the kinetic of two regions is different?

Previously, it is confirmed that the reaction between Li and Si can be divided into two regions, R1(O1) and R2(O2), from the thermodynamic experiments and other research papers. Then, how the kinetic of two regions, R1(O1) and R2(O2), would be different? To check this, commercial nano-Si electrodes are tested with various current densities, 400, 800, 1600, 2400, 3200 mA g^{-1}, and investigate how the current densities affect to the lithiation/delithiation profiles.(Figure 3.9) The voltage window for this experiment is also confined to 0.06 to 1.5 V to avoid crystallization of *a*-Li_xSi at low voltage.

In lithiation/delithiation profiles in Figure 3.10, the tendency for profiles to shift to the direction of larger overpotential region is observed as the current densities increase. It can be understood by increased *iR* drop as current densities increase, but, there are other possibilities, such as limited utilization of active materials due to increased current densities. So, to confirm this, differential capacity profiles are calculated, and depicted in Figure 3.11.

In Figure 3.11, the separated peaks of R1(O1) and R2(O2) are found. By the way, the interesting point is that the tendencies of R1(O1) and R2(O2) for

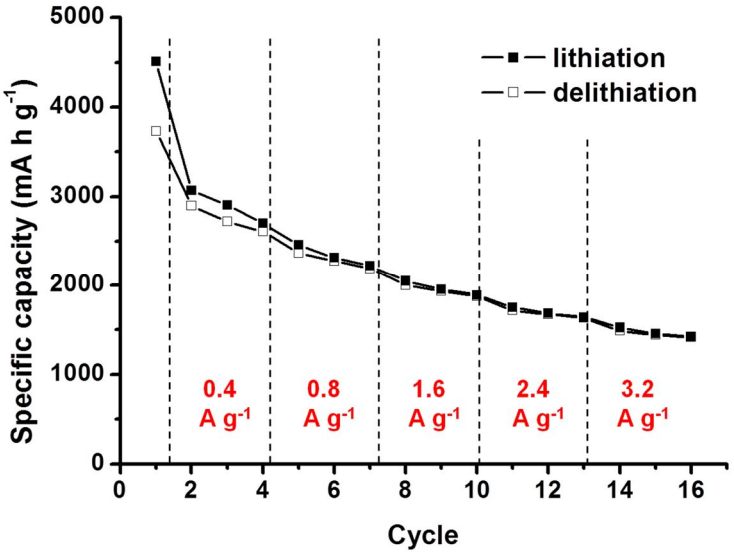

Figure 3.9. Rate performance of nano-Si.

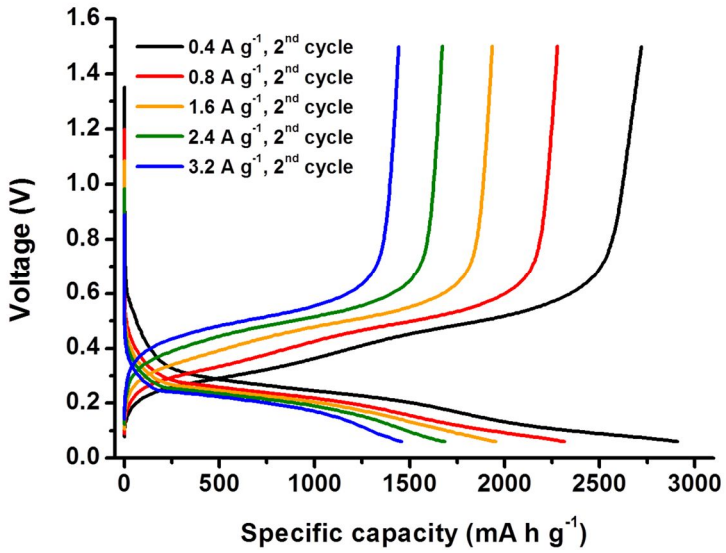

Figure 3.10. Lithiation/delithiation profiles of nano-Si with various current densities.

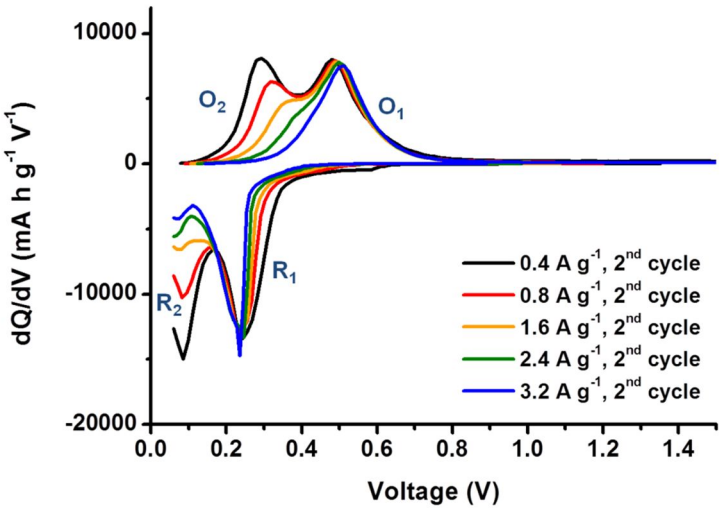

Figure 3.11. Differential capacity profiles of nano-Si with various current densities.

responding to increasing current densities. In the case of R1(O1), the amount of change in the peak positions along the current densities is not that large. Instead, the peaks become slim as current density increases. It reveals that the resistance related to R1(O1) is small, but as the current density increases, the reaction time is reduced, resulting in less utilization of active material. On the other hand, the peak position of R2(O2) responds to the current density subtly, resulting in large dependency of capacity from R2(O2) to the current densities. It means that the resistance related to R2(O2) is large.

The R1 and R2 peaks are hard to deconvolute due to cut-off voltage nearby, so, delithiation profiles in Figure 3.11 are deconvoluted and their peak positions are depicted along the current densities in Figure 3.12. It shows that the peak position of O2 responds to current densities more sensitively than that of O1. According to ohm's law, $R = \frac{V}{I}$, the slope of peak position change along the current density means resistance, R. Therefore, it could be concluded that O2 has larger reaction resistance than O1, which is consistent with the trend in R1 and R2. Larger resistance of R2 can be affected by R1; when Si reacts with Li, volume expansion is accompanied, therefore, R1 can affect R1. To confirm effect of current densities on R2 without the effect of R1, thus, 400 mA g^{-1} is applied to 0.12 V, followed various current densities are applied to 0.06 V. (Figure 3.13) Furthermore, it is checked whether

R1(O1) and R2(O2) are maintained along the cycles or not. (Figure 3.14) Along the cycles with 400 mA g^{-1}, R1(O1) and R2(O2) are maintained, therefore, use R1(O1) and R2(O2) for analyzing the kinetics of Si is reasonable. Furthermore, slow kinetics of R2 without the effect of R1 is re-confirmed.

To analyze these resistances in detail, EIS experiment was conducted using symmetric cells. The representative potentials for EIS experiments were chosen where the peak potential is; 0.25 V for R1, 0.08 V for R2, 0.30 V for O2, and 0.50 V for O1. The impedance data and equivalent circuit for fitting

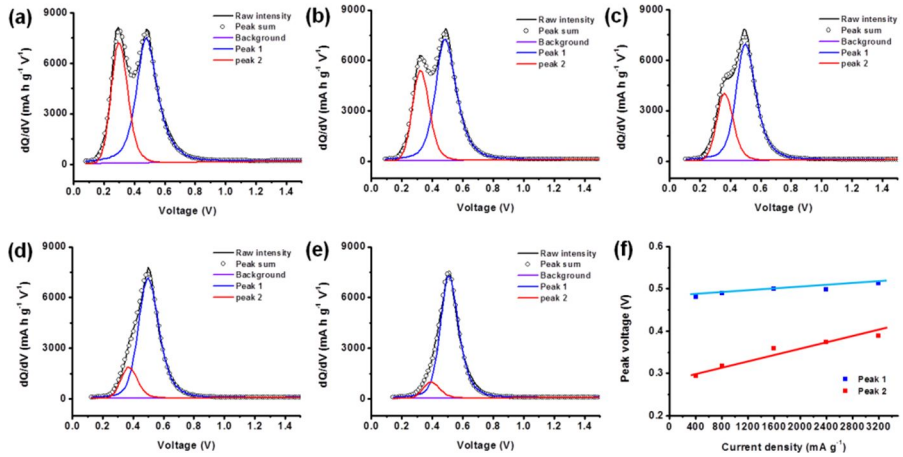

Figure 3.12. Peak deconvolution of differential capacity profiles at different current densities: (a) 400, (b) 800, (c) 1600, (d) 2400, (e) 3200 mA g^{-1}, (f) peak potential profile at different current densities

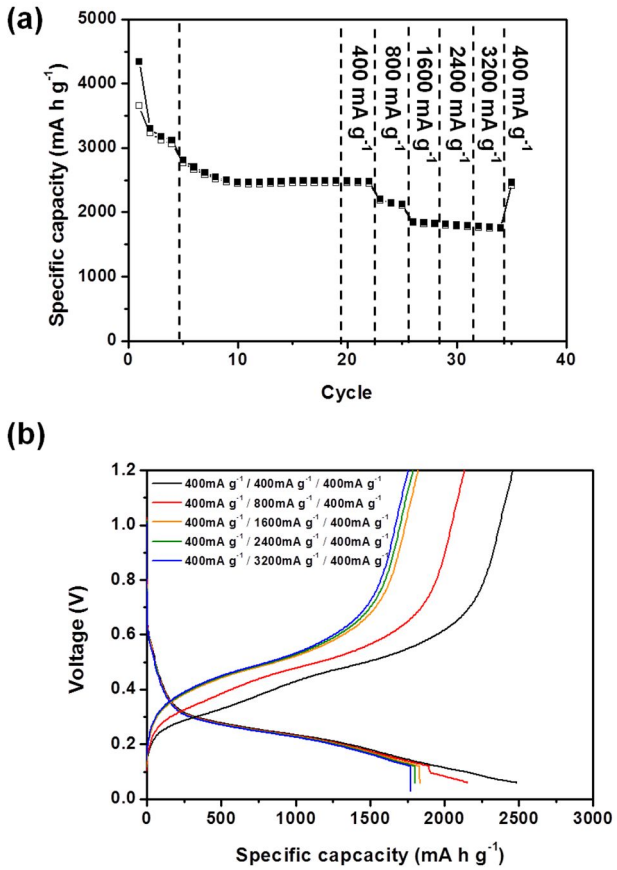

Figure 3.13. (a) Power performance and (b) its charge/discharge profiles; 400 mA g^{-1} is applied until 0.12 V and various current densities are applied to 0.06 V.

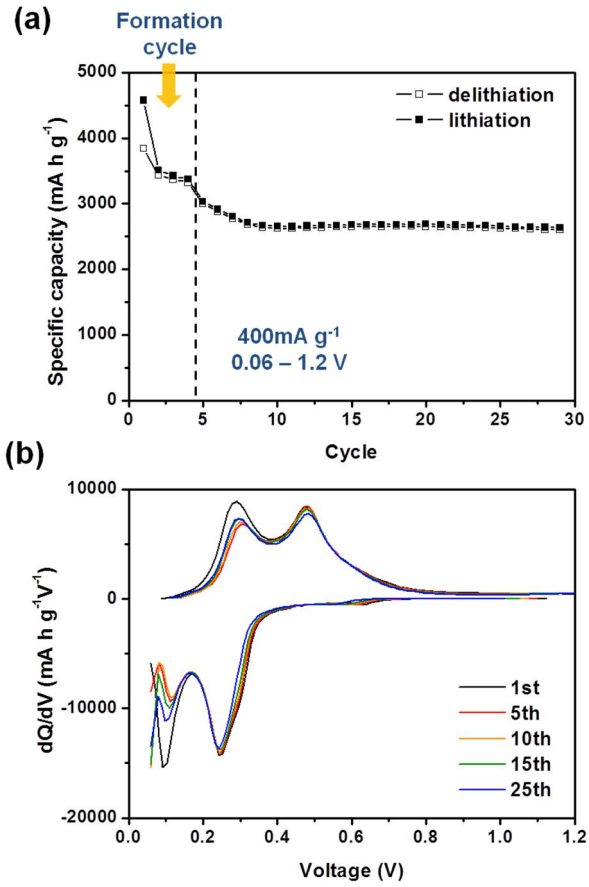

Figure 3.14. (a) Cycle performance of Si with constant current density, 400 mA g^{-1} and (b) its differential capacity profiles along the cycles. Formation cycles were performed at first 4 cycles; 1.2 to 0.01 V.

are shown in Figure 3.15, and the fitted data is tabulated in Table 3.1. Before analyzing the impedance data, let's understand the equivalent circuit minutely. The equivalent circuit in Figure 3.15 is composed of three RC circuits; the first RC circuit stands for solid-electrolyte interphase (SEI) part, second RC circuit stands for charge transfer part, and final part stands for unknown part.[78] The physical meaning of the third RC circuit is still unknown, but, accuracy of fitting is enhanced surprisingly. Y. Cui group also found this phenomena, and also applied this term to fitting impedance data.[79] Then, let's compare the impedance data for R1 and R2. R_{sei} and R_{ct} in R2 are larger than that of R1. This is consistent with the fact that R1 has faster kinetics than the case of R2, as shown in differential capacity profiles. Furthermore, the third semicircle, which stands for unknown part, for R2 is also larger than that for R1. Based on the information above, faster kinetics for R1 can be temporarily rationalized. When the impedances for O1 and O2 are compared, however, they were contradicted with the case of R1 and R2; R_{sei} and R_{ct} for O2 is smaller than that for O1. If R_{sei} and R_{ct} can account for the kinetics shown in the differential capacity profiles, R_{sei} and R_{ct} for O2 should also have be larger than that for O1. Therefore, it could be concluded that R_{sei} and R_{ct} from impedance data are not the parameters that determine the kinetics of R1(O1) and R2(O2). Then, why R_{sei} and R_{ct} showed such a

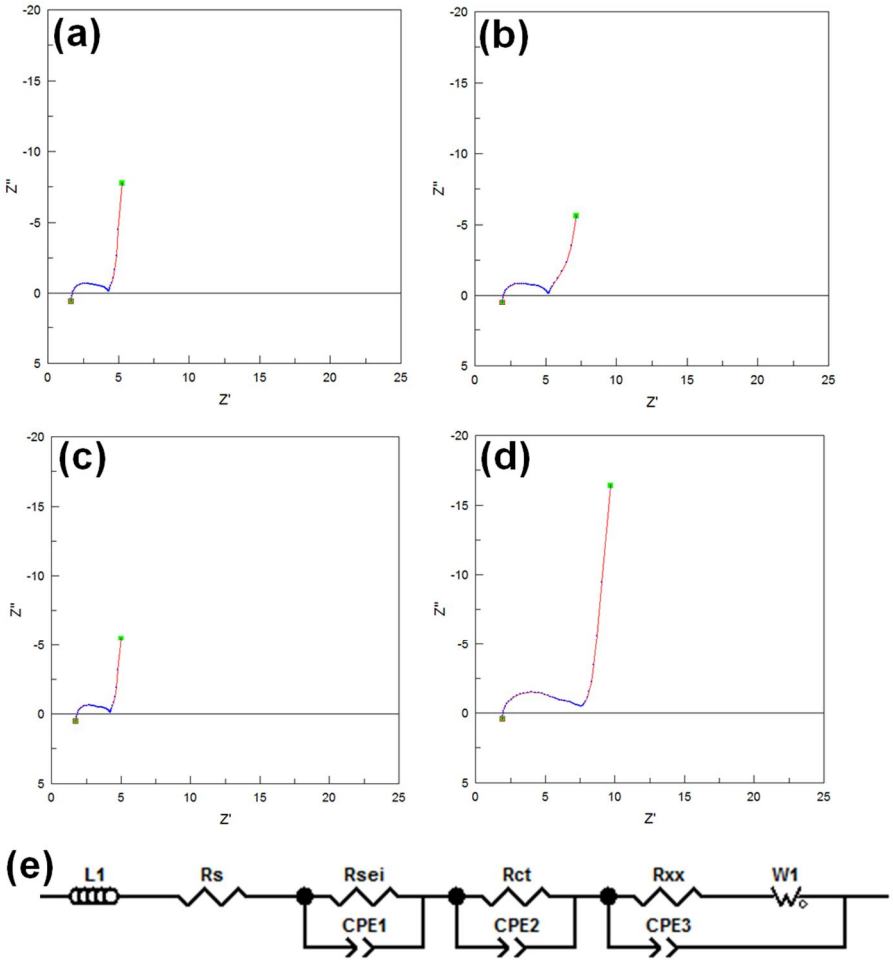

Figure 3.15. EIS data with various conditions; (a) 0.25 V, (b) 0.08 V in lithiation, (c) 0.3 V, (d) 0.5 V. (e) Equivalent circuit used in this study.

Table3.1. The fitting results from equivalent circuit.

Sample name	0.25 V (R1)	0.08 V (R2)	0.3 V (O2)	0.5 V (O1)
R_{sei}	1.52	1.87	1.42	3.32
R_{ct}	1.27	1.50	1.15	2.89
R_{xx}	1.18	4.62	-	-

contradicting trend in R1/R2 and O1/O2? To understand this phenomena, the models of lithiation and delithiation are depicted in Figure 3.16 using the concept of two-phase reaction as confirmed above. (The lithiation product of R1, which has relatively small amout of Li is named to '*a*-Li_xSi', and the lithiation product of R2, which has relatively large amount of Li is named to '*a*-Li_ySi', $x < y$)

In the first lithiation region, R1, the reaction between two phases, *a*-Si and *a*-Li_xSi, is progressed by two-phase reaction. At this moment, inner part of the active material is *a*-Si, and outer part of the active material is *a*-Li_xSi. After R1 and short transition state (region B), which is progressed by solid-solution reaction, two-phase reaction between *a*-$Li_{x+\delta}Si$ and *a*-Li_ySi is followed. In this reaction, inner part of the active material is *a*-$Li_{x+\delta}Si$, and outer part of the active material is *a*-Li_ySi. This trend in lithiation is also observed in delithiation inversely. In first delithiation process, O2, inner part of active material is *a*-Li_ySi and outer part of active material is *a*-$Li_{x+\delta}Si$. And inner part of active material is *a*-Li_xSi and outer part of active material is *a*-Si in second lithiation process, O1. When this trend is combined with electric conductivities of each phase, the trend of R_{ct} can be accounted.

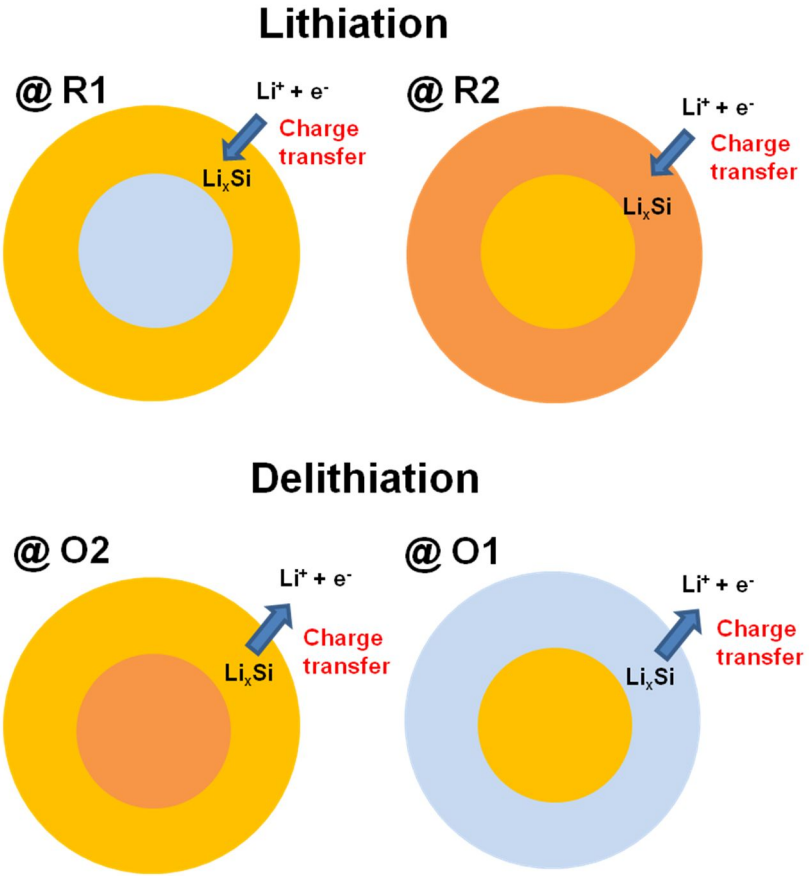

Figure 3.16. The predicted reaction model along the lithiation / delithiation.

According to D. Aurbach group, the change of electric conductivity along lithiation and delithiation is as follows [80]: the electric conductivity increases along the progress of R1, and the electric conductivity decreases along the progress of R2. From this information, electric conductivity of each phase can be inferred as follow:

$$\sigma_{a-\mathrm{Li}_x\mathrm{Si}} > \sigma_{a-\mathrm{Li}_y\mathrm{Si}} > \sigma_{a-\mathrm{Si}}$$

where, σ is electric conductivity. This trend can be also checked in delithiatoin process. In many researches, electric conductivity is related to R_{ct}.[81,82] Therefore, the information above reflect the electric conductivity for outer part of active material is related to R_{ct}.

R_{sei} is the resistance related to the transport of Li ion through SEI layer. Some groups reported that low or high potentials, which is harsh condition for stability of SEI layer or electrolyte, transforms the composition or structure of SEI layer, and it makes hard for Li ion to transport through SEI layer. [79,83] Thus, larger R_{sei} in R2 and O1 than that in R1 and O2 can be accounted by structure and composition change of SEI layer along the potentials.

Therefore, the electric conductivity of outer part of active material and the composition and structure of SEI layer affect to R_{ct} and R_{sei}, but, they are not direct parameters that affect kinetics of R1(O1) and R2(O2). Furthermore,

rationalization the difference in kinetics just by the size of semicircles in impedance data is dangerous.

Then, what is major parameter that determine the kinetics of R1(O1) and R2(O2)? The possible candidate is diffusion in bulk active material; Li ion diffusion or phase boundary movement. Many research reported that the rate determining step for the active material with two-phase reaction is phase boundary movement. The indirect evidence for slow phase boundary movement is the appearance of third semicircle at low frequency in R2. The element that affects to impedance at such a low frequency region is change of crystallite structure.[84] Therefore, there is possibility that R2 may proceed with structural change. But, the origin of semicircle in impedance at low frequency can be accounted by other reasons, therefore, further works to verify the origin of this semicircle is necessary.

3.3.3. Application

Using the information acquired above, the strategies are discussed to use Si more effectively. The result of the experiment on kinetics is that the kinetic of R1(O1) is faster than that of R2(O2). Based on this result, I suggest that using only R1 part of Si with appropriate size, rather than using with complex nano-structured Si; the proper size, which is free from pulverization along the lithation, is reported around hundreds of nanometer-size.[85] Such limited utilization of appropriate size of Si can avoid the problems related to nano-structured Si with large surface area and large voltage window;

1. Save trouble for making a complicate nano-structured material.
2. Avoid large amount irreversible capacities originated from the large surface area, such as SEI layers.
3. High cut-off voltage.in this case, 0.1 V, can prevent Li plating on active material.
4. Faster kinetics of R1 is favorable even at high current densities.
5. Limited utilization of Si can alleviate severe volume expansion, which can be result in degradation of electrode, therefore, it has advantage on cycle retention.
6. Small surface area can reduce the amount of unnecessary SiO_2.

Figure 3.17 shows the result of rate performance for commercial nano-Si with cut-off voltage between 0.1 and 1.2 V and nano-structured Si with cut-off voltage between 0.01 and 1.2 V. In the case of 400 mA g^{-1}, the difference in capacity between two different cut-off voltages is large due to absence of R2 utilization. On the other hand, when current density increases to 1600 mA g^{-1}, the difference in capacity decreases, because R2 utilization is decreased even at large voltage range. Furthermore, when cycles are performed at a constant high current density, 1600 mA g^{-1}, Si with 0.1 to 1.2 V cut-off range showed better retention compared with that of 0.01 to 1.2 V. It means that narrow voltage range can relief damages on electrode. Therefore, limited utilization of commercial nano-Si can alleviate cell degradation due to large volume expansion along the cycle.

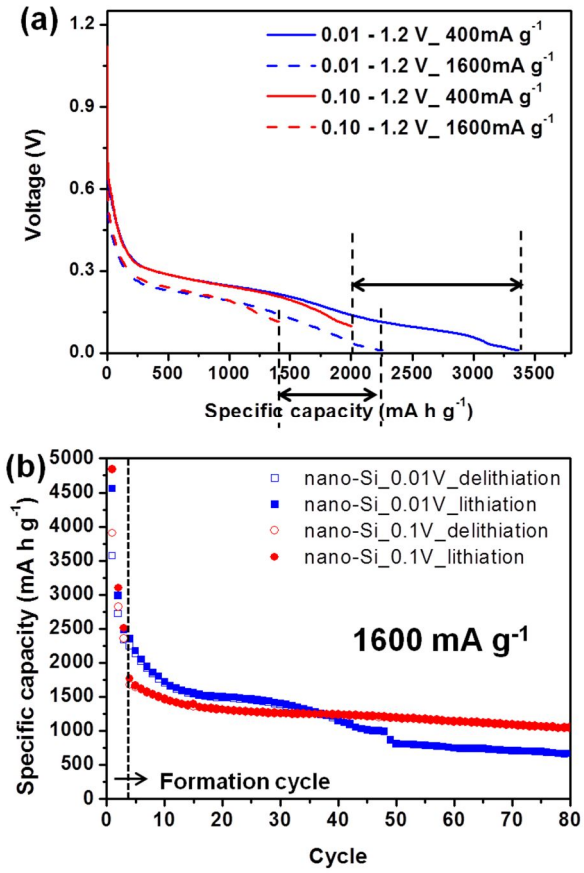

Figure 3.17. The electrochemical performances of commercial nano-Si with voltage window of 0.1 to 1.2 V and 0.01 to 1.2 V. (a) Discharge profiles with different current densities, 400 mA g^{-1} and 1600 mA g^{-1}. (b) Cycle performance of Si with constant current density, 1600 mA g^{-1}.

3.4. Conclusion

In this study, the reaction mechanism of Li-Si system is investigated by observing the variation of OCVs along the temperatures and depth of lithiations. Using thermodynamic relations, the entropy changes along the reaction is studied, and concluded that Li-Si system is progressed with two-phase reaction, which is opposite from the understanding so far. Two sloping regions and transition region connecting these two sloping regions in lithiation/delithiation profile are tried to be explained by Gibbs free energy graph. Other evidences, such as the existence of the regions where show lower orders of magnitude for diffusion coefficient, and the fact that suitable explanation is possible with two-phase reaction than solid-solution reaction, are also support our assertion.

Furthermore, the reaction kinetics of R1(O1) and R2(O2) is confirmed with electrochemical analysis, such as differential capacity profiles, and EIS. R1(O1) shows faster kinetics than R2(O2). The origin of this phenomena seems to be slow phase boundary movement in R2(O2); the resistances related to charge transfer and SEI layer cannot explain appropriately. Due to the lack of direct evidence that reveals slow phase boundary movement in R2(O2), however, further works is necessary.

Using the information acquired above, the electrochemical tests with

reduced voltage window are conducted to use Si more effectively. It shows that the cells with reduced voltage window also have comparable capacity to the cells with nano-structured Si with traditional voltage window. Furthermore, effective utilization is also possible even at high current densities due to fast kinetics of R1(O1).

These results give the insight that the deep understanding of reaction mechanism and kinetics can help us to establish a strategy to use an active material more effectively.

References

[1] M.S. Islam, and C.A. Fisher, Lithium and sodium battery cathode materials: computational insights into voltage, diffusion and nanostructural properties, Chem. Soc. Rev., **2014**, 43, 185-204.

[2] M.R. Palacin, Recent advances in rechargeable battery materials: a chemist's perspective, Chem. Soc. Rev., **2009**, 38, 2565-2575.

[3] R. Yazami, and P.H. Touzain, A reversible graphite-lithium negative electrode for electrochemical generators, J. Power Sources, **1983**, 9, 365-371.

[4] K. Mizushima, P.C. Jones, P.J. Wiseman, J.B. Goodenough, Li_xCoO2 ($0<x<1$): A new cathode material for batteries of high energy density, Mater. Res. Bull., **1980**, 15, 783-789.

[5] D.J. Kim, J.W. Choi, Lithium-ion Batteries: Present and Future, 물리학과 첨단기술, **2012**, Jan./Feb. 15-19.

[6] V. Etacheri, R. Marom, R. Elazari, G. Salitra, and D. Aurbach, Challenges in the development of advanced Li-ion batteries: a review, Energy Environ. Sci., **2011**, 4, 3243-3262.

[7] E. Buiel, and J.R. Dahn, Li-insertion in hard carbon anode materials for Li-ion batteries, Electrochim. Acta, **1999**, 45, 121-130.

[8] Y.-M. Lin, P.R. Abel, D.W. Flaherty, J. Wu, K.J. Stevenson, A. Heller, and ClB. Mullins, Morphology dependence of the lithium storage capability and rate performance of amorphous TiO_2 electrodes, J. Phys. Chem. C, **2011**, 115, 2585-2591

[9] B. Koo, H. Xiong, M.D. Slater, V.B. Prakapenka, M. Balasubramanian, P. Podsiadlo, C.S. Johnson, T. Rajh, and E.V. Shevchenko, Hollow Iron Oxide Nanoparticles for Application in Lithium Ion Batteries, Nano Lett., **2012**, 12, 2429-2435.

[10] C.K. Chan, H. Peng, G. Liu, K. McIlwrath, X.F. Zhang, R.A. Huggins, and Y. Cui, High-performance lithium battery anodes using silicon nanowires, Nature nanotechnol., **2008**, 3, 31-35.

[11] K.T. Nam, D.-W. Kim, P.J. Yoo, C.-Y. Chiang, N. Meethong, P.T. Hammond, Y.-M. Chiang, and A.M. Belcher, Virus-Enabled Synthesis and Assembly of Nanowires for Lithium Ion Battery Electrodes, Science, **2006**, 312, 885-888.

[12] P.L. Taberna, S. Mitra, P. Poizot, P. simon, and J.-M. Tarascon, High rate capabilities Fe_3O_4-based Cu nano-architectured electrodes for lithium-ion battery applications, Nature Mater., **2006**, 5, 567-573.

[13] T.H. Hwang, Y.M. Lee, B.-S. Kong, J.-S. Seo, and J.W. Choi, Electrospun Core–Shell Fibers for Robust Silicon Nanoparticle-Based Lithium Ion Battery Anodes, Nano Lett., **2012**, 12, 802, 807.

[14] J. Jiang, Y. Li, J. Liu, and X. Huang, Building one-dimensional oxide nanostructure arrays on conductive metal substrates for lithium-ion battery anodes , Nanoscale, **2011**, 3, 45-58.

[15] Y. Yu, L. Gu, C. Zhu, S. Tsukimoto, P,A. Aken, and J. Maier, Reversible Storage of Lithium in Silver-Coated Three-Dimensional Macroporous Silicon, Adv. Mater., **2010**, 22, 2247-2250.

[16] J.-M. Jeong, B.G. Choi, S.C. Lee, K.G. Lee, S.-J. Chang, Y.K. Han, Y.B. Lee, H.U. Lee, S. Kwon, G. Lee, C.-S. lee, and Y.S. Huh, Adv. Mater., **2013**, 25, 6250-6255.

[17] Z. Wang, D. Luan, F.Y.C. Boey, and X.W. Lou, Fast Formation of SnO_2 Nanoboxes with Enhanced Lithium Storage Capability, J. Am. Chem. Soc. **2011**, 133, 4738-4741.

[18] X.W. Lou, C. Yuan, and L.A. Archer, Double-Walled SnO_2 Nano-Cocoons with Movable Magnetic Cores, Adv. Mater., **2007**, 19, 3328-3332.

[19] W. Wang, and P.N. Kumta, ACS Nano, **2010**, 4, 2233-2241.

[20] H. Zhang, P.V. Braun, Three-Dimensional Metal Scaffold Supported Bicontinuous Silicon Battery Anodes, Nano Lett., **2012**, 12, 2778-2783.

[21] M. Yoshio, H. Wang, K. Fukuda, T. Umeno, N. Dimov, and Z. Ogumi, Carbon-coated Si as a lithium ion battery anode material, J. Electrochem. Soc., **2002**, 149, A1598-A1603.

[22] J. Luo, X. Zhao, J. Wu, H.D. Jang, H.H. Kung, and J. Huang, Crumpled Graphene-Encapsulated Si Nanoparticles for Lithium Ion Battery Anodes, J. Phys. Chem. Lett., **2012**, 3, 1824-1829..

[23] S.-H. Yu, X. Guo, D. Ling, D.Y. Chung, A. Jin, M. Shokouhimehr, T. Hyeon and Y.-E. Sung, Facile synthesis of nanostructured carbon nanotube/iron oxide hybrids for lithium-ion battery anodes, RSC Adv., **2014**, 4, 37365-37370.

[24] K.J. Lee, S.-H. Yu, J.-J. Kim, D.-H. Lee, J. Park, S.S. Suh, J.S. Cho, and Y.-E. Sung, $Si_7Ti_4Ni_4$ as a buffer material for Si and its electrochemical study for lithium ion batteries, J. Power Sources, **2014**, 246, 729-735.

[25] H. Han, T. Song, E.-K Lee, A. Devadoss, Y. Jeon, J. Ha, Y.-C Chung, Y.-M Choi, Y.-G. Jung, and U. Paik, "Dominant factors governing the rate capability of a TiO2 nanotube anode for high power lithium ion batteries", ACS Nano, **2012**, 6, 8308-8315.

[26] T. Xia, W. Zhang, J. Murowchick, G. Liu and X. Chen, Built-in Electric Field-Assisted Surface-Amorphized Nanocrystals for High-Rate Lithium-Ion Battery, Nano Lett., **2013**, 13, 5289-5296.

[27] X. Wang, S. Qiu, G. Lu, C. He, J. Liu, L. Luan, and W. Liu, Fabrication of porous MnO microspheres with carbon coating for lithium ion battery application, CrystEngComm., **2014**, 16, 1802-1809.

[28] H. Chen, Q. Zhang, J. Wang, D. Xu, X. Li, Y. Yang, and K. Zhang, Improved lithium ion battery performance by mesoporous Co_3O_4 nanosheets grown on self-standing $NiSi_x$ nanowires on nickel foam, J. Mater. Chem. A, **2014**, 2, 8483-8490.

[29] E. Kang, Y.S. Jung, G.-H. Kim, J. Chun, U. Wiesner, A.C. Dillon, J.K. Kim and J. Lee, Highly Improved Rate Capability for a Lithium-Ion Battery Nano-$Li_4Ti_5O_{12}$ Negative Electrode via Carbon-Coated Mesoporous Uniform Pores with a Simple Self-Assembly Method, Adv. Func., Mater., 2011, 21, 4349-4357.

[30] J. Jin, S.-Z. Huang, J. Liu, Y. Li, D.-S. Chen, H.-E. Wang, Y. Yu, L.-H. Chen, and B.-L. Su, Design of new anode materials based on hierarchical,

three dimensional ordered macro-mesoporous TiO_2 for high performance lithium ion batteries, J. Mater. Chem. A, **2014**, 2, 9699-9708.

[31] P.-Y. Chang, C.-H. Huang, and R.-A. Doong, Ordered mesoporous carbon-TiO_2 materials for improved electrochemical performance of lithium ion battery, Carbon, **2012**, 50, 4259-4268.

[32] R.A. Huggins 저, 강기석 역, 배터리:재료과학의 고급이해, 1st Ed., 홍릉과학출판사, Chapter 2.

[33] D.R. Gaskell, Introduction to the thermodynamics of materials, 5th Ed., Taylor and Francis, Chapte 10..

[34] W. Fan, M. A. Snyder, S. Kumar, P.-S. Lee, W. C. Yoo, A. V. McCormick, R. L. Pennm A. Stein and M. Tsapatsis, Hierarchical nanofabrication of microporous crystals with ordered mesoporosity, Nature Mater., **2008**, 7, 984-991.

[35] P.-S. Lee, X. Zhang, J. A. Stoeger, A. Malek, W. Fan, S. Kumar, W. C. Yoo, S. A. Hashimi, R. L. Penn, A. Stein, and M. Tsapatsis, Sub-40 nm zeolite suspensions via disassembly of three-dimensionally ordered mesoporous-imprinted silicate-1, J. Am. Chem. Soc., **2011**, 133, 493-502.

[36] T. Yokoi, Y. Sakamoto, O. Terasaki, Y. Kubota, T. Okubo and T. Tatsumi, Periodic arrangement of silica nanospheres assisted by amino acids, J. Am. Chem. Soc., **2006**, 128, 13664-13665.

[37] B. T. Yonemoto, Q. Guo, G. S. Hutchings, W. C. Yoo, M. A. Snyder and F Jiao, Structural evolution in ordered mesoporous TiO_2 anatase electrodes, Chem. Commun., **2014**, 50, 8997-8999.

[38] M. A. Reddy, V. Pralong, U. V. Varadaraju and B. Raveau, Crystallite size constraints on lithium insertion into brookite TiO_2, Electrochem. Solid-State Lett., **2008**, 11, A132-A134.

[39] C. Jiang, M. Wei, Z. Qi, T. Kudo, I. Honma and H. Zhou, Particle size dependence of the lithium storage capability and high rate performance of nanocrystalline anatse TiO_2 electrode, J. Power Sources, **2007**, 166, 239-243.

[40] M. Wagemaker, W. J. H. Borghols and F. M. Mulder, Large impact of particle size on insertion reactions. A case for anatase Li_xTiO_2, J. Am. Chem. Soc., **2007**, 129, 4323-4327.

[41] A. V. Ven, J. Bhattacharya and A. A. Belak, Understanding Li diffusion in Li-intercalation compounds, Acc. Chem. Res., **2013**, 46, 1216-1225.

[42] J.-Y. Shin, D. Samuelis and J. Maier, Sustained lithium-storage performance of hierarchical, nanoporous anatase TiO2 at high rates: emphasis on interfacial storage phenomena, Adv. Funct., Mater., **2011**, 21, 3464-3472.

[43] M. Wagemaker and F. M. Mulder, Properties and promise of nanosized insertion materials for Li-ion batteris, Acc. Chem. Res., **2013**, 46, 1206-1215.

[44] J. Maier, Thermodynamic aspects and morphology of nano-structured ion conductors: Aspect of nano-ionics Part 1, Solid State Ionics, **2002**, 154-155, 291-301.

[45] J. Jamnik and J. Maier, Nanocrystallinity effects in lithium battery materials: Aspects of nano-ionics Part IV, Phys. Chem. Chem. Phys., **2003**, 5, 5215-5220.

[46] V. Subramanian, H. Zhu, R. Vajtai, P. M. Ajayan and B. Wei, Hydrothermal synthesis and pseudocapacitance properties of MnO2 nanostructures, J. Phys. Chem. B, **2005**, 109, 20207-20214.

[47] J. Wang, J. Polleux, J. Lim and B. Dunn, Pseudocapacitive contributions to electrochemical energy storage in TiO_2 (Anatase) nanoparticles, J. Phys. Chem. B, **2007**, 111, 14925-14931.

[48] J. Jin. S.-Z. Huang, J. Liu, Y. Li, D.-S. Chen, H.-E. Wang, Y. Yu, L.-H. Chen and B.-L. Su, Design of new anode materials based on hierarchical, three dimensional ordered macro-mesoporous TiO_2 for high performance lithium ion batteries, J. Mater. Chem. A, **2014**, 2, 9699-9708.

[49] J.-Y. Luo, Y.-G. Wang, H.-M. Xiong and Y.-Y. Xia, Ordered mesoporous spinel $LiMn_2O_4$ by a soft-chemical process as a cathode material for lithium-ion batteries, Chem. Mater., **2007**, 19, 4791-4795.

[50] M. Karthik, E. Redondo, E. Goikolea, V. Roddatis, S. Doppiu and R. Mysyk, Effect of mesopore ordering in otherwise similar micro/mesoporous carbon on the high-rate performance of electric double-layer capacitors, J. Phys. Chem. C, **2014**, 118, 27715-27720.

[51] Y. Aihara, S. Arai and K. Hayamizu, Ionic conductivity, DSC and self diffusion coefficient of lithium, anion, polymer, and solvent of polymer gel electrolytes: The structure of the gels and the diffusion mechanism of the ions, Electrochim. Acta, **2000**, 45, 1321-1326.

[52] A. J. Bard and L. R. Faulkner, Electrochemical methods: Fundamentals and applications, Wiley, River Street, Honoken, NJ, U.S.A., 2001.

[53] H. S. Fogler, Elements of chemical reaction engineering, Pearson, Upper Saddle River, NJ, U.S.A., 2005.

[54] S. K. Bhatia, M. R. Bonilla and D. Nicholson, Molecular transport in nanopores: a theoretical perspective, Phys. Chem. Chem. Phys., **2011**, 13, 15350-15383.

[55] M. Stempniewicz, M. Rohwerder and F. Marlow, Release from silica SBA-3-like mesoporous fibers: cross-wall transport and external diffusion barrier, ChemPhysChem., **2007**, 8, 188-194.

[56] Y. Fu, F. Ye, W. G. Sanders, M. M. Collinson and D. A. Higgins, Single molecule spectroscopy studies of diffusion in mesoporous silica thin films, J. Phys. Chem. B, **2006**, 110, 9164-9170.

[57] V. T. Hoang, Q. Huang, M. Eic, T. O. Do and S. Kaliaguine, Structure and diffusion characterization of SBA-15 materials, Langmuir, **2005**, 21, 2051-2057.

[58] C. Hellriegel, J. Kirstein and C. Brauchle, Tracking of single molecules as a powerful method to characterize diffusivity of organic species in mesoporous materials, New J. Phys., 2005, 7, 23.

[59] R.A. Huggins 저, 강기석 역, 배터리:재료과학의 고급이해, 1st Ed., 홍릉과학출판사, Chapter 7.

[60] Y. Iijima, Y. Takahashi, K.I. Matsumoto, T. Hayashi, N. Todoroki, T. Wadayama, Oxygen reduction reaction activities of Pt/Au(1 1 1) surfaces prepared by molecular beam epitaxy, J. Electroanal. Chem., **2012**, 685, 79-85.

[61] Wei-Jun Zhang, Lithium insertion/extraction mechanism in alloy anodes for lithium-ion batteries, J. Power Sources, **2011**, 196, 877-885..

[62] J. Li, A. Smith, R.J. Sanderson, T.D. Hatchard, R.A. Dunlap, and J.R. Dahn, In situ Mossbauer effect study of the reaction of lithium with Si using a Sn probe, J. Electrochem. Soc,, **2009**, 156, A283-A288..

[63] G. Zhou, D.-W. Wang, F. Li, L. Zhang, N. Li, Z.-S. Wu, L.Wen, G. Qing, and H.-M. Cheng, Graphene-wrapped Fe3O4 anode material with improved reversible capacity and cyclic stability for lithium ion batteries, Chem. Mater., **2010**, 22, 5306-5313.

[64] R. Meduri, C. Pendyala, V. Kumar, G.U. Sumanasekera, and M.K. Sunkara, Hybrid tin oxide nanowires as stable and high capacity anodes for Li-ion batteries, Nano Lett., **2009**, 9, 612-616.

[65] S. Han, B. Jang, T. Kim, S.M. Oh, and T. Hyoen, Simple synthesis of hollow tin dioxide microspheres and their application to lithium-ion battery anodes, Adv. Func., Mater., **2005**, 15, 1845-1850.

[66] T.D. Hatchard, and J.R. Dahn, In situ XRD and electrochemical study of the reaction fo lithium with amorphous silicon, J. Electrochem. Soc., **2004**, 151, A838-A842.

[67] H. Tan, A study of the thermodynamics and kinetics of LixFePO4 as a cathode material fo rLi batteries, Ph.D. Thesis, **2012**, Caltech..

[68] Y. F. Reynier, R. Yazami, and B. Fultz, Thermodynamics of lithium intercalation into graphites and disordered carbons, Journal of

Electrochemical Society, **2004**, 151, A422-A426.

[69] Y. F. Reynier, R. Yazami, and B. Fultz, The entropy and enthalpy of lithium intercalation into graphite, Journal of Power Sources, **2003**, 119-121, 850-855.

[70] K. Takano, Y. Saito, K. Kanari, K. Nozake, K. Kato, A. Negishi and T. Kato, Entropy change in lithium ion cells on charge and discharge, Journal of Applied Electrochemistry, **2002**, 32, 251-258.

[71] B. Key, M. Morcrette, J.-M. Tarascon, and C.P. Grey, Pair distribution function analysis and solid state NMR studies of silicon electrodes for lithium ion batteries: Understanding th e(de)lithiation mechanism, JACS, **2011**, 133, 506-512.

[72] B. Key, R. Bhattacharyya, M. Morcrette, V. Seznec, J.-M. Taraston, and C.P. Grey, Real-time NMR investigations of structural changes in silicon electrodes for lithium-ion batteries, JACS, **2009**, 131, 9239-9249.

[73] W. Weppner, and R.A. Huggins, Determination of the kinetic parameters of mixed-conducting electrodes and application to the system Li_3Sb, J. Electrochem. Soc., **1977**, 124, 1569-1578.

[74] Y. Zhu, and C. Wang, Galvanostatic Intermittant Titration Technique for Phase-Transformation Electrodes, Journal of Physical Chemistry C, **2010**, 114, 2830-2841.

[75] P.P. Prosini, M. Lisi, D. Zane, and M. Pasquali, Determination of the chemical diffusion coefficient of lithium in $LiFePO_4$, Solid State Ionics, **2002**, 148, 45-51.

[76] J. Xie, N. Imanishi, T. Zhang, A. Hirano, Y. Takeda, and O. Yamamoto, Li-ion diffusion kinetics in $LiFePO_4$ thin film prepared by radio frequency magnetron sputtering, Electrochimica Acta, **2009**, 54, 4631-4637.

[77] Y. Rho, and K. Kanamura, Li^+ ion diffusion in $Li_4Ti_5O_{12}$ thin film electrode prepared by PVP sol-gel method, Journal of Solid State Chemistry, **2004**, 177, 2094-2100.

[78] M. Dolle, F. Orsini, A.S. Gozdz, and J.-M. Tarascon, Development of reliable three-electrode impedance measurements in plastic Li-ion batteries, J. Electrochem. Soc., **2001**, 148, A851-A857.

[79] R. Ruffo, S.S. Hong, C.K. Chann, R.A. Huggins, and Y. Cui, Impedance analysis of silicon nanowire lithium ion battery anode, J. Phys. Chem. C, **2009**, 113, 11390-11398.

[80] E. Pollak, G.Salitra, V. Baranchugov, and D. Aurbach, In situ conductivity, impedance spectroscopy, and ex situ raman spectra of amorphous silicon during the insertion/extraction of lithium, J. Phys. Chem. C, **2007**, 111, 11437-11444.

[81] C.H. Chen, J. Liu, and K. Amine, Symmetric cell approach and impedance spectroscopy of high power lithium-ion batteries, J. Power Sources, **2001**, 96, 321-328.

[82] P.Arora, B.N. Popov, and R.E. White, Electrochemical investigations of cobalt-doped $LiMn_2O_4$ as cathode materials for lithium-ion batteries, J. Electrochem. Soc., **1998**, 145, 807-815.

[83] Y.M. Lee, J.Y. Lee, H.-T. Shim, J.K. Lee, and J.-K. Park, SEI layer formation on amorphous Si thin electrode during precycling, J. Electrochem. Soc., **2007**, 154, A515-A519.

[84] E. Barsoukov, J. R. Macdonald, Impedance spectroscopy: Theory, experimental, and applications, 2nd Ed., Wiley, Chaper 4.

[85] Z. Ma, T. Li, Y.L. Huang, J. Liu, Y. Zhou, and D. Xue, Critical silicon-anode size for averting lithiation –induced mechanical failure of lithium-ion batteris, RSC Adv., **2013**, 3, 7398-7402.

국문초록

리튬이온전지 음극 물질인 티타늄 산화물과 실리콘의 속도론과 반응 메커니즘

리튬이온전지는 양극과 음극에서의 가역적인 전기화학반응을 이용하여 전기에너지를 화학에너지로 저장 또는 화학에너지를 전기에너지로 변환하는 에너지 저장·변환 장치이다. 지금까지의 리튬이온전지는 소형 IT 기기의 에너지원으로 사용되는 등 제한된 영역에서 주로 사용되었다. 하지만 앞으로는 전기자동차나 에너지 저장 시스템의 저장소 등 좀 더 넓은 범위에서 사용될 가능성이 있고, 이 때문에 리튬이온전지의 에너지 밀도나 출력특성을 높이기 위한 연구가 활발히 진행되고 있다. 이를 위해 에너지 밀도가 높은 물질, 예를 들어 실리콘과 같은 리튬 합금 물질이 효과적으로 사용되기 위한 방법이나, 구조 또는 전기전도도 향상을 통해 출력특성을 높이기 위한 방법들이 주로 연구되었다. 하지만 에너지 밀도가 높은 물질을 효과적으로 사용하거나 출력특성을 향상시키기 위해서는 해당 물질의 반응 메커니즘을 좀 더 깊이 이해하거나, 출력특성에 영향을 미치는 요소들을 세분화하여 각각의 영향을 독립적으

로 관찰할 필요가 있는데, 이러한 연구들은 아직 많지 않다.

이 연구에서는 먼저 출력특성을 결정하는 한 요소인 전해질에서의 이온 이동을 연구하였다. 리튬염 이동이 용이하다고 알려진 메조 다공성 구조를 갖는 티타늄 산화물을 모델 시스템으로 정하였는데, 티타늄 산화물은 리튬과의 반응에 부피가 크게 변하지 않기 때문에 부피 팽창이라는 변수를 제거할 수 있어 리튬염의 이동만 관찰하기에 유리하다. 나노 실리카를 형판으로 하여 구멍 크기와 입자 크기가 서로 다른 다섯 종류의 3차원 규칙적인 메조 다공성 구조를 갖는 티타늄 산화물을 합성하였고, 이를 투과전자현미경, x-선 회절 분석기, 저각 x-선 회절 분석기, 질소 흡착 장비 등을 이용하여 구조 분석을 진행하였다. 그리고 이를 활물질로 이용하여 전기화학 실험을 진행하였는데, 보통 사용되는 1 몰농도의 전해질에서는 합성된 물질 사이의 전기화학 성능에 차이가 없었지만, 0.1 몰농도의 묽은 전해질에서는 입자 크기에 따라 입자 내부에서 리튬염이 고갈되는 현상이 확인되었다. 그리고 구멍의 크기가 클수록 리튬염의 고갈이 더 높은 전류밀도에서 나타남을 확인하였다. 실험을 통해 얻은 결과를 이용하여, 티엘 수를 변수로 갖는 수학적 모델을 세울 수 있었고, 이 모델을 이용하여 다양한 크기와 더 넓은 범위의 전류밀도에서 리튬염의 고갈이 일어날 지점을 예측하였다.

연구의 나머지 부분에서는, 높은 이론 용량을 갖는 음극 물질

인 실리콘의 반응 메커니즘과 속도론을 연구하였다. 지금까지 실리콘은 고용체 반응을 통해 리튬과 반응한다고 알려졌지만, 최근 2상 반응을 통해 리튬과 반응한다는 연구가 발표되며, 그 반응 메커니즘에 대해 논란이 있었다. 하지만, 실리콘과 리튬이 반응할 때 실리콘의 결정구조가 무너져 비정질로 변하기 때문에 기존의 분석 방법으로는 반응 메커니즘을 확인하기 어려움이 있다. 이 연구에서는 전기화학 방법과 열역학 관계식을 이용하여 실리콘과 리튬의 반응을 분석하였고, 그 결과, 실리콘과 리튬은 비정질 상태에서도 두 단계의 2상 반응을 통해 반응이 진행됨을 확인하였다. 그리고 실리콘 내부에서 리튬 양에 따른 리튬의 확산계수가 갖는 경향성과 열역학적 이해를 통해, 실리콘과 리튬의 반응이 고용체 반응보다 2상 반응이 더 논리적으로 어울림을 보였다. 더 나아가, 다양한 전류밀도를 이용하여 실리콘의 전기화학 실험을 진행하였고, 이를 통해 두 단계의 2상 반응이 서로 다른 속도로 일어남을 확인하였다. 두 단계의 2상 반응이 다른 속도로 일어나는 원인을 전기화학 임피던스 분석 방법을 이용하여 전하전달저항과 고체 전해질 계면상 필름저항으로 분리하여 분석하였고, 그 결과 위 두 저항이 반응의 속도를 결정하는 것이 아님을 확인하였다. 속도를 결정하는 단계를 크게 세 가지로 나눌 수 있는데, 위 분석들을 통해 실리콘과 리튬의 반응은 주로 고체 내부에서의 이온 확산 속도로 결정될 것

이라는 잠정적인 결론을 내렸다. 느린 리튬 이온 확산은 실리콘과 리튬의 반응이 구조적 변화를 동반하기 때문으로 추측하였다. 그리고 이를 바탕으로 실리콘을 좀 더 효과적으로 이용할 수 있는 방법, 전위 창 및 입자 크기 조절을 제안하였고, 이를 실험적으로 확인하였다.

이 연구를 통해 활물질의 반응 메커니즘을 분석하였고, 물질이 적용되는 전류 밀도의 범위에 따라 어떤 요소가 좀 더 고려되어야 할지에 대한 이해를 할 수 있었는데, 이러한 정보들은 활물질을 좀 더 효과적으로 사용할 수 있는 전략을 제시하는 바탕이 될 수 있다는 점에서 의미를 갖는다.

주요어: 리튬이온전지, 리튬염 이동, 실리콘, 반응 메커니즘, 속도론.

학번: 2009-23953